THE JOURNAL OF PHYSICAL CHEMISTRY C
A JOURNAL OF THE AMERICAN CHEMICAL SOCIETY

pubs.acs.org/JPCC

Article

Coadsorbed Species with Halide Ligands on Silver Nanoparticles with Different Binding Affinities

Published as part of The Journal of Physical Chemistry virtual special issue "Nanophotonics for Chemical Imaging and Spectroscopy".

Yi Zhang,* Sujay Prabakar, and Eric C. Le Ru

Cite This: *J. Phys. Chem. C* 2022, 126, 8692–8702

Read Online

ACCESS | Metrics & More | Article Recommendations | Supporting Information

ABSTRACT: Understanding ligand binding on silver nanoparticles (AgNPs) is crucial regarding its behavior in photocatalytical and bioanalytical applications. However, the preferentially adsorbed species on AgNPs and their relative binding affinities are uncertain when halide ligands are involved. Herein, we demonstrate the variations in the adsorbed species on citrate-reduced AgNPs upon ligand exchange to Cl^-, Br^-, and I^- and propose a mechanism based on surface-enhanced Raman spectroscopy (SERS) results. When Cl^- is introduced to the AgNPs, citrate anion desorbs, but its decomposition product, acetoacetate (AAc^-), is relatively preferred for coadsorption. When the halide ligands are bulkier (Br^- or I^-), AAc^- is also displaced due to stronger repulsion, while residual anionic surfactants (AS) can bind to the AgNPs presumably through the gaps between the bulky halide ions. Further, the above-mentioned coadsorbed species are present together with a cationic protein (type I collagen). AS persist in their coadsorption when I^- ligands coat the AgNPs, resulting in the interference SERS spectra of AS overlapping with collagen. In contrast, collagen outperforms AS on Br^- ligand coated AgNPs, and thus, no interference was observed. This study will bring attention to the potential pitfalls during precise surface functionalization of AgNPs or other plasmonic nanostructures for interfacial properties and applications.

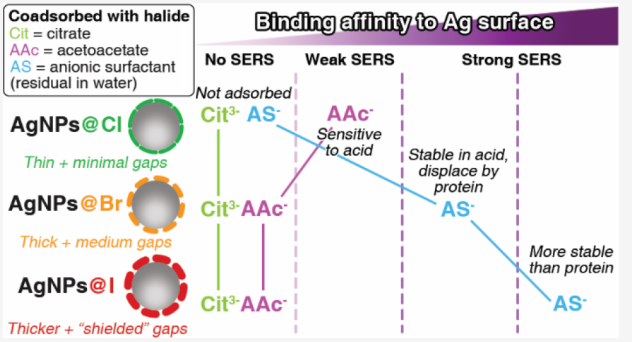

INTRODUCTION

Dating back to the 4th century, silver nanoparticles (AgNPs) were used in decoration for their exceptional optical properties when sized at nanoscale.[1] A similar phenomenon was discovered in gold nanoparticles (AuNPs) by Faraday in the 19th century[2] and later explained by the Mie scattering theory.[3] Nowadays, AgNPs are used in a broad range of applications in which their surface chemistry and near-field properties are crucial for their performances.[4−9] In a highly recognized method of synthesizing AgNPs,[10] sodium citrate is used as both a reducing agent and a capping ligand to give a monodispersed, stable colloidal solution. The as-prepared surface layer of citrate is often exchanged by other ligands to provide specific functionalities in need of various applications.[9,11−13]

While the formation of a complete coating layer over the AgNPs upon ligand exchanges with halides (Cl^-, Br^-, and I^-) has been widely accepted,[14−16] evidence that contradicts such an assumption is not rare.[17−21] However, the opinions emerging from this evidence were divergent. A tentative assignment of the coadsorbed species on I^- ligand coated AuNPs to polyvinylpyrrolidone (PVP) by Huang et al.[17] was later corrected to citrate anions by Xie et al. and Park et al., based on similar experiments in which they exposed AuNPs to I^- and thiols, respectively.[18,19] On the contrary, Perera et al. found that halides and thiol ligands can readily eliminate citrate anions but leave unspecified organic cations on AuNPs.[20] Recently, Wang et al. observed the coadsorption of an unspecified surface anion with Br^- and trace amounts of fentanyl on AgNPs.[21] The existing evidence is inconclusive for depicting a mechanism of the coadsorption and, more importantly, the binding affinities of the species on different ligand coated AgNPs. Clarifying the coadsorption mechanism of citrate, halides, and other species on the AgNPs is crucial to many applications that rely on the surface properties, including photocatalysis,[22] bioanalysis,[23] and therapeutics.[7]

Received: February 14, 2022
Revised: April 27, 2022
Published: May 12, 2022

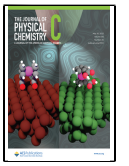

https://doi.org/10.1021/acs.jpcc.2c01092
J. Phys. Chem. C 2022, 126, 8692−8702

Previous studies on the adsorption of ligands with AgNPs were conducted using a range of techniques, including transmission electron microscopy (TEM),[24] X-ray photoelectron spectroscopy (XPS),[20,25,26] Fourier-transform infrared spectroscopy (FT-IR),[19,25,26] second harmonic generation (SHG),[27] UV−vis spectroscopy,[28,29] and surface-enhanced Raman spectroscopy (SERS).[20,30−33] In particular, SERS was recently used to study the binding of citrate and other bound species on AuNPs for its advantages in directly probing the molecular vibrational modes at an enhanced resolution originating from the surface plasmon resonance (SPR).[20,33]

Here, using SERS, we investigate the changes in the coadsorbed species on citrate-reduced AgNPs when Cl^-, Br^-, and I^- ligand exchanges take place and propose a mechanism explaining these observations. Our results suggest the presence of coadsorbed species on the AgNPs even after allowing sufficient time and concentration for halide ligand exchanges; however, the preferred species are different when the ligand changes from Cl^- to Br^- or I^-. Further evidence of the competition between the species and protein to coadsorb with halide ligands on AgNPs emphasizes the determinative role of the halide ligands on the varied binding affinity of the species, which also highlights the complexity of bioanalytical scenarios in general. This study not only provides a thorough understanding of the binding interactions of AgNPs with citrate, halides, proteins, and other soluble species but also illustrates a novel way to reveal the surface chemistry of plasmonic NPs for the precise control of functionalities in photocatalytical, bioanalytical, and medical applications.

EXPERIMENTAL SECTION

Materials. Trisodium citrate dihydrate ($Na_3C_6H_5O_7{\cdot}2H_2O$ or $Na_3Cit{\cdot}2H_2O$, Pure Science Ltd., New Zealand), silver nitrate ($AgNO_3$, Apollo Scientific Ltd., UK), hydroxylamine hydrochloride ($NH_2OH{\cdot}HCl$, Sigma-Aldrich, US), potassium chloride (KCl, Pure Science Ltd., New Zealand), potassium bromide (KBr, Merck KGaA, Germany), potassium iodide (KI, Sigma-Aldrich, US), sodium hydrosulfide hydrate (NaHS, Sigma-Aldrich, US), hydrochloric acid (HCl, CARLO ERBA Reagents S.r.l., Italy), sodium hydroxide (NaOH, CARLO ERBA Reagents S.r.l., Italy), sodium acetate trihydrate ($CH_3COONa{\cdot}3H_2O$, $NaAc{\cdot}3H_2O$, Pure Science Ltd., New Zealand), and magnesium sulfate ($MgSO_4$, Fisher Chemical, UK) were purchased and used without further purification. A collagen solution was prepared following the procedures reported elsewhere,[34] while replacing 0.5 M acetic acid by 5 mM HCl to avoid interference from its methyl ($-CH_3$) and carboxyl (−COOH) groups.

Synthesis of the AgNPs. Lee-Meisel's method[10] was followed for synthesizing citrate-reduced AgNPs. A mixture of 3.3 mL of 0.5% (w/v) silver nitrate and 94 mL of DI water was heated to boiling. Then, 3.0 mL of 1% (w/v) $Na_3Cit{\cdot}2H_2O$ was rapidly added to the boiling mixture. The mixture was kept boiling under vigorous stirring for 1 h and then cooled down to room temperature. The green-gray cloudy solution was transferred to a Schott bottle and topped up to 100 g with DI water. The solution was stored at 4 °C and kept away from light.

Leopold's method[35] was followed for synthesizing hydroxylamine-reduced, citrate-free h-AgNPs. An initial mixture of 3.0 mL of 100 mM NaOH, 10.0 mL of $NH_2OH{\cdot}HCl$, and 77 mL of DI water was prepared at room temperature. Then, under vigorous stirring, 10.0 mL of 10 mM $AgNO_3$ was added dropwise to the mixture. The dropwise addition took about 1 to 2 min to finish, and the mixture was kept stirring for another 10 min. The yellow-gray cloudy solution was then transferred to a Schott bottle, stored at 4 °C, and kept away from light.

Both methods produce polydisperse, polycrystalline AgNPs with characterizations shown in Figure S1.

Centrifugation, Ligand Exchange, and Aggregation of the AgNPs. The preparation methods for key samples of this study are briefly described below in three steps. A full list of sample preparation methods is shown in Table S1.

1 Centrifugation: In a 1.5 mL Eppendorf tube (Protein LoBind), 1000 μL of AgNPs was centrifuged at 5 krpm for 15 min. After centrifugation, 900 μL was removed from the supernatant, and the remaining 100 μL was redispersed using a vortex mixer at a low speed at 200 rpm for 1 s.
2 Ligand exchange: To the concentrated 100 μL of AgNPs was added 100 μL of 5 mM KCl (or 1 mM KBr or 1 mM KI), and the mixture was incubated at room temperature for 5 min ($[Cl^-]_{final}$ = 1.25 mM, calculated as in the 400 μL final mixture, same below; $[Br^-]_{final}$ = 0.25 mM; $[I^-]_{final}$ = 0.25 mM).
   An alternative route in the ligand exchange step was followed for introducing citrate and its decomposition products to h-AgNPs, for the investigation of bound species on AgNPs@Cl. To the concentrated 100 μL of h-AgNPs was added 65 μL of heat decomposed 2 mM Na_3Cit and 35 μL of 10 mM KCl, and the mixture was incubated at room temperature for 5 min ($[Cl^-]_{final}$ = 1.25 mM, equivalent $[Cit]_{eq,\ final}$ = 0.325 mM). Heat decomposition of Na_3Cit was carried out by keeping 1 mL of a 2 mM Na_3Cit solution in a 1.5 mL Eppendorf tube at 95 °C for 3 h.
3 Aggregation: The resulting 200 μL solution was mixed with 200 μL of 5 mM $MgSO_4$ (or 5 mM $MgSO_4$ in 2 mM HCl or 50 μg/mL collagen in 2 mM HCl), to form the 400 μL final aggregated mixture.

SERS/Raman Measurements. SERS spectra of AgNP solutions were measured using a Horiba Jobin-Yvon LabRam HR spectrometer equipped with a Symphony CCD detector cooled with liquid N_2 at −130 °C, in a backscattering configuration through a LM Plan FI Olympus air objective (×50, NA = 0.50) by focusing at 300 μm below the solution/air interface. Excitation was provided by a 514 nm argon-ion laser (Melles-Griot) at around 10 mW for an exposure time ranging from 3 to 10 s, with 10 accumulations. Each sample was around 200 μL and was contained in the cap of the Eppendorf tube of the corresponding sample to avoid cross contamination. Raman spectra of collagen film were measured using the same setup but with a laser focusing around 20 μm above the solid/air interface (defocused)[36] to reduce the fluorescence from solid collagen. Flat-field correction was carried out to minimize the static features from the notch filter and the response of the CCD (see the SI for details). The intensity of each Raman spectrum is normalized to count per second and stacked by offsetting (or scaling when indicated).

RESULTS AND DISCUSSION

Without Halide Ligand Exchange (AgNPs@Cit): The Adsorption of Citrate. Lee-Meisel's protocol is known to produce AgNPs with an adsorbed citrate layer (AgNPs@Cit), although oxidative and thermal decomposition products of

https://doi.org/10.1021/acs.jpcc.2c01092
J. Phys. Chem. C 2022, 126, 8692−8702

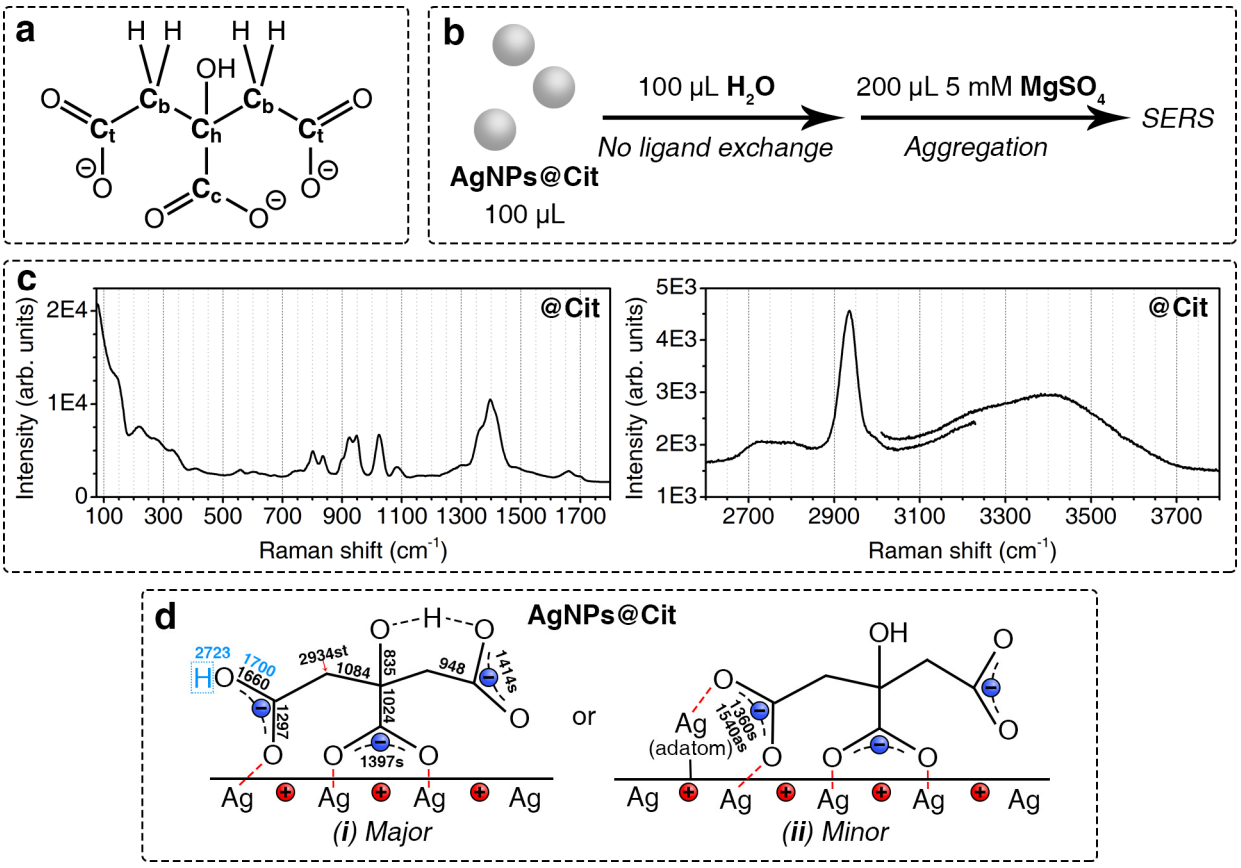

Figure 1. (a) Structure of the citrate anion with notation for each carbon atom (t = terminal carboxyl, c = central carboxyl, h = hydroxyl, b = bridge). (b) Sample preparation steps for AgNPs@Cit. (c) SERS spectra of AgNPs@Cit aggregated using $MgSO_4$. Note that the two spectra from 2600 to 3800 cm^{-1} are not superimposed, as they were measured at different grating positions (same below). (d) Possible binding coordinations of citrate with Ag atoms. Associated SERS peaks (in cm^{-1}) from citrate are attached to the bonds. The red arrow indicates the $-CH_x-$ group vibrations. The blue colored text highlights the partial protonation of citrate and the related SERS peaks. Notations (same below): s = symmetric stretching, as = asymmetric stretching, st = stretching, d = scissoring, w = wagging.

citrate are also present in the final solution.[37] To record the SERS spectra of the bound citrate with sufficient resolution, the AgNPs@Cit are concentrated by centrifugation and aggregated using $MgSO_4$ (Figure 1b). (Note that $MgSO_4$ would not displace the adsorbed citrate from AgNPs, as SO_4^{2-} has a much weaker binding affinity to Ag atoms compared to citrate.[31]) The acquired spectrum (Figure 1c) shows characteristic citrate SERS peaks at 2934 ($\nu_s(CH_2)$), 2723 (ν(O−H), in κ^1-COOH), 1700sh ($\nu(C_t-OH)$, κ^1-C_tOOH) (sh = shoulder; see notation of carbon atoms (C_x) in Figure 1a, same below), 1660 ($\nu(C_t{=}O)$, κ^1-C_tOO^-), 1414sh ($\nu_s(COO^-)$, unbound), 1397 ($\nu_s(C_cOO^-)$, bound), 1360sh ($\nu_s(C_tOO^-)$, bound), 1297w ($\nu(C_t-O)$, κ^1-C_tOO^- or κ^1-C_tOOH) (w = weak), 1084 ($\nu(C_b-C_h)$), 1024 ($\nu(C_c-C_h)$, bound), 948 ($\nu(C_t-C_b)$, unbound), 925 ($\nu(C_t-C_b)$, bound), 899sh (ν(C−COO)), and 835 cm^{-1} ($\nu(C_h-O)$), in addition to a broad peak at 218 cm^{-1} assigned to ν(COO−Ag), indicating the binding of citrate via its carboxyl ($-COO^-$) group (Table S2, sample 2-1-1).[33,37−42] The binding coordination of citrate in AgNPs@Cit resembles the citrates on the rough surfaces of AuNPs (with adatoms), highlighted by the prominent 1084 cm^{-1} peak of $\nu(C_b-C_h)$ that indicates at least one terminal carboxyl ($-C_tOO^-$) group and the central carboxyl ($-C_cOO^-$) group in citrate are bound to the Ag atoms (Figure 1d).[33,43]

Cl^- Ligand Exchange (AgNPs@Cl): The Desorption of Citrate and the Coadsorption of Acetoacetate (AAc) with Cl^- Ligands. Upon mixing with Cl^- (AgNPs@Cl, $[Cl^-]_{final}$ = 1.25 mM) and aggregated using $MgSO_4$ (Figure 2a), a weak SERS spectrum is observed (Figure 2c, green). In addition to the peak at 239 cm^{-1} (ν(Ag−Cl))[13] showing the direct binding of Cl^- to Ag atoms, other peaks are identified at 2935, 2849, 1610, 1436sh, 1398w, 1299w, 1098vw, 1128, 1062w, 926w, and 889w cm^{-1} (Table S3, sample 3-1-3). These peaks are not affected with further increases in Cl^- concentration or time allowed for ligand exchange (the maximum $[Cl^-]_{final}$ = 2.5 mM, time increases from 5 to 60 min, Figure S3). Therefore, despite the opposite claims elsewhere,[29,44] our results imply that, although Cl^- ligands form a near-complete layer, a considerable amount of Ag atoms remains exposed for direct binding with species.

A straightforward assumption for the bound species is citrate in a different coordination, since the spectrum of AgNPs@Cl seems to match most of the citrate peaks from AgNPs@Cit, but the minor differences are of concern. A new peak at 2849 cm^{-1} is revealed as the intensity of the 2935 cm^{-1} peak diminishes. The peak at 2935 cm^{-1} was previously observed in bound citrate;[38,39] however, the 2849 cm^{-1} peak was scarcely reported. Interestingly, the 2935 and 2849 cm^{-1} peaks can also be observed with a higher speed centrifugation with no addition of KCl nor aggregation using $MgSO_4$ (Figure S4,

https://doi.org/10.1021/acs.jpcc.2c01092
J. Phys. Chem. C 2022, 126, 8692−8702

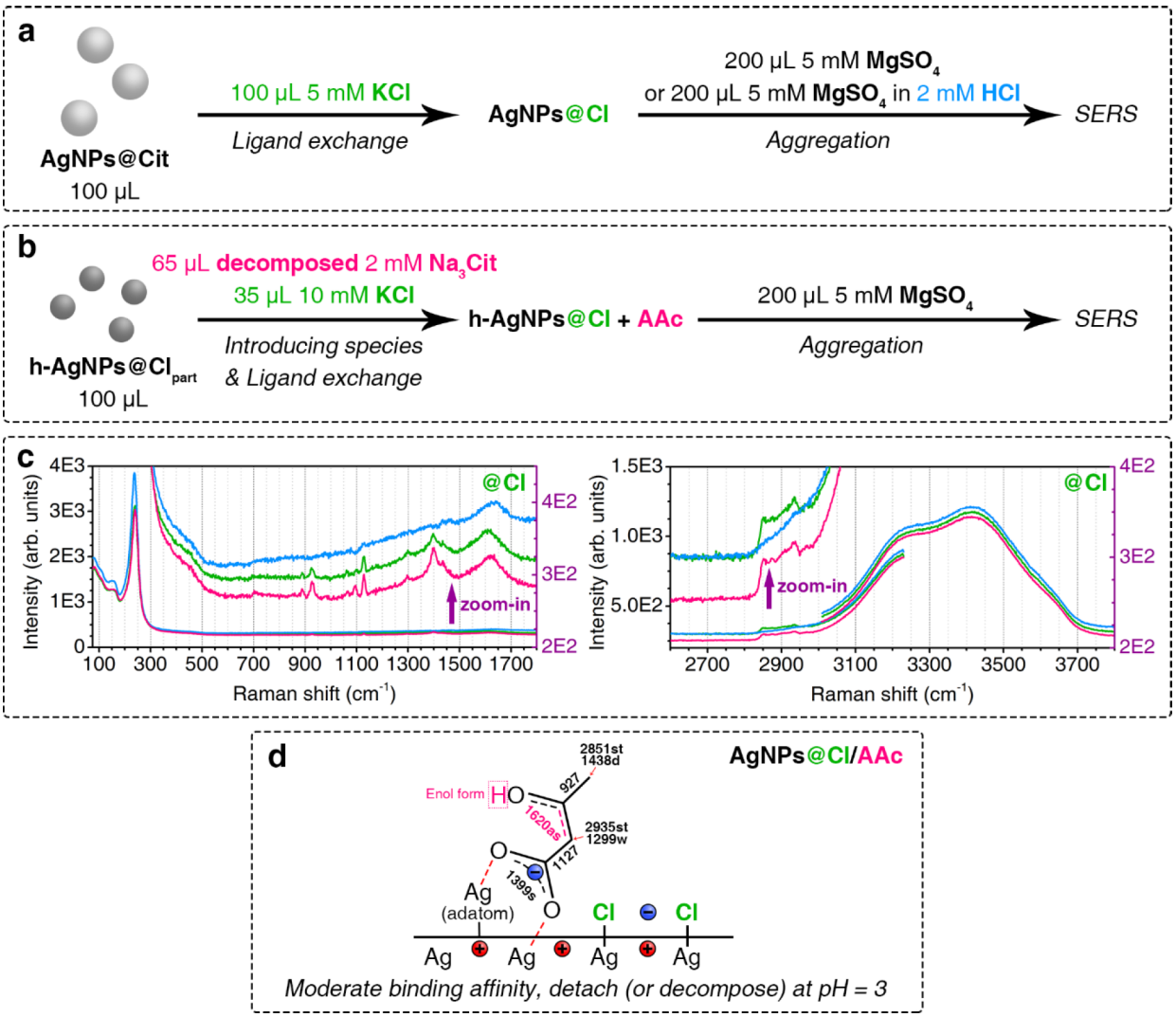

Figure 2. (a, b) Sample preparation steps for AgNPs@Cl and h-AgNPs@Cl + AAc. (c) Stacked SERS spectra of AgNPs@Cl aggregated using $MgSO_4$ (green) or using HCl acidified $MgSO_4$ (blue). Full scale spectra (follow left *y*-axes) were displayed to show the Ag−Cl peak below 300 cm^{-1}, whereas weak features are highlighted by zooming in the same spectra (indicated by the purple arrow), with *y*-axes on the right side for the scales. (d) Possible binding coordinations of AAc with exposed Ag atoms on AgNPs@Cl. Associated SERS peaks (in cm^{-1}) from AAc are attached to the bonds (The red arrow indicates the $-CH_x-$ group vibrations.). The pink colored text highlights the enol form of AAc and the related SERS peaks.

sample 1-1-3). This could suggest that the species is also adsorbed onto AgNPs@Cit before Cl^- ligand exchange takes place.

For further investigation, a citrate-free synthesis of AgNPs (h-AgNPs) was carried out, and the NPs were aggregated using $MgSO_4$. The h-AgNPs have an intrinsic layer of Cl^- (h-AgNPs@Cl_{part}) introduced during the synthesis by the reducing agent $NH_2OH{\cdot}HCl$. Although the existing Cl^- concentration ($[Cl^-]_{final}$ = 0.375 mM) is much lower than that in AgNPs@Cl ($[Cl^-]_{final}$ = 1.25 mM), a clean spectrum was observed after $MgSO_4$ aggregation, with no evident peaks except the ν(Ag−Cl) and water peaks (Figure S4, sample 3-3-1). This observation confirms that those peaks in AgNPs@Cl are relevant to citrate or its decomposition products.

To differentiate citrate from its decomposition products, fresh Na_3Cit at different concentrations ($[Cit]_{final}$ = 0.25 to 2.5 mM) was added to the h-AgNPs@Cl_{part}, followed by the aggregation using $MgSO_4$ (Figure S5). The SERS spectra of fresh Na_3Cit are observed and are different from the spectrum of AgNPs@Cl, showing peaks at 2937vw ($\nu_s(CH_2)$), 1622 ($\nu_{as}(COO^-)$), 1415sh ($\nu_s(COO^-)$, unbound), 1373 ($\nu_s(C_tOO^-)$, bound), 1028 ($\nu(C_c-C_h)$), 951 ($\nu(C_t-C_b)$, unbound), 923 ($\nu(C_t-C_b)$, bound), 899sh ($\nu(C-COO)$), and 833w cm^{-1} ($\nu(C_h-O)$),[33,37,38,41] in addition to the strong ν(Ag−Cl) peak at 240 cm^{-1} (Table S2, sample 3-5-3).[13] However, when we add extra KCl into the mixture of Na_3Cit and h-AgNPs@Cl_{part} to match the Cl^- concentration in AgNPs@Cl, the above peaks disappear (Figure S6). The absence of citrate signals suggests that the electrostatic repulsion of Cl^- and citrate anions counteracts the affinity of citrate anions to coadsorb with Cl^-. Hence, the whole spectrum with the 2849 cm^{-1} peak can only be attributed to the decomposition products of citrate. The decomposition products of citrate were investigated in previous studies. Munro et al. investigated the SERS spectra of acetonedicarboxylic acid (H_2ADC) and acetoacetic acid (HAAc) on AgNPs, and later, Grys et al. measured ADC^{2-}, AAc^-, and acetate (Ac^-) on AuNPs.[33,37]

https://doi.org/10.1021/acs.jpcc.2c01092
J. Phys. Chem. C 2022, 126, 8692−8702

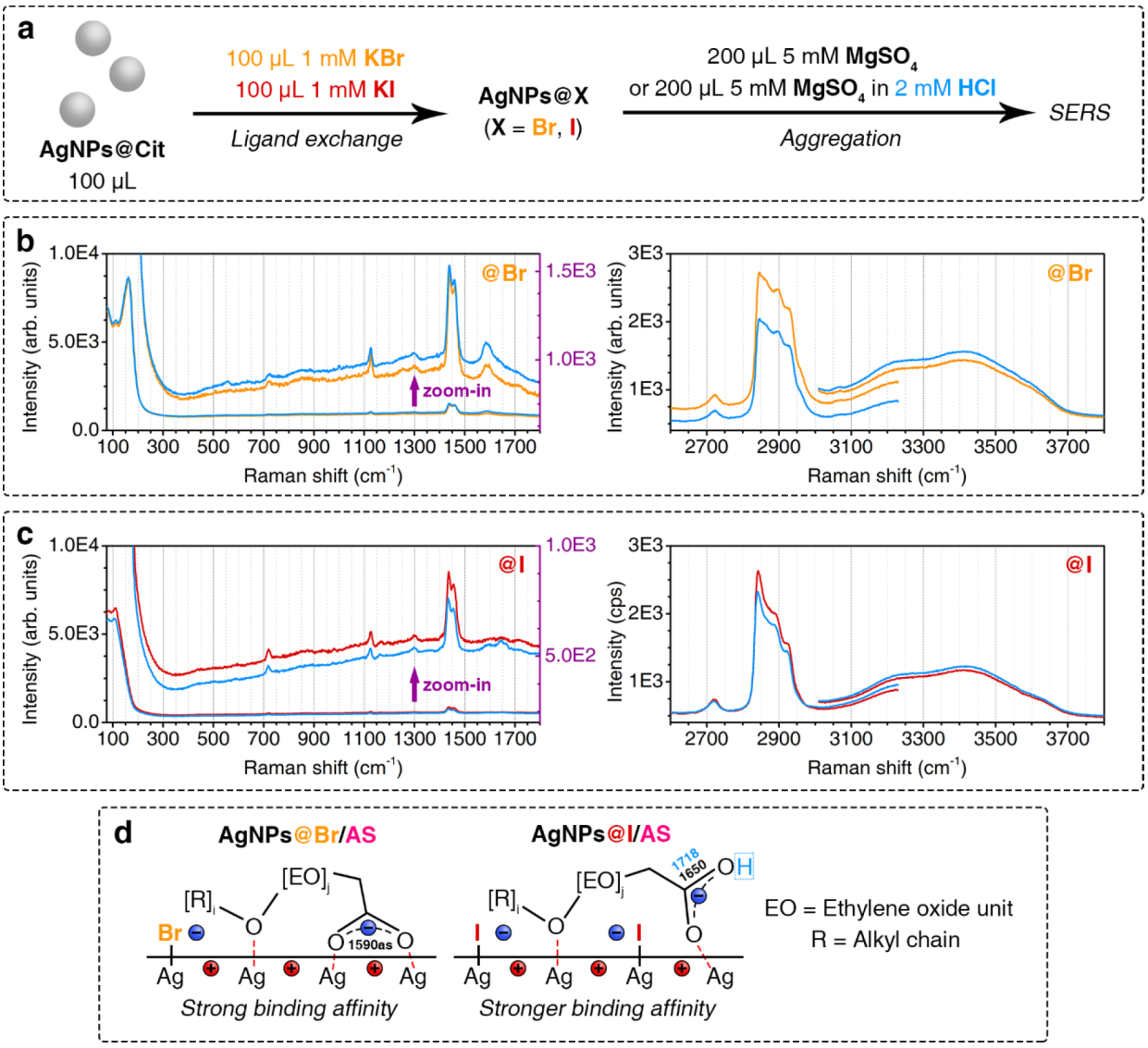

Figure 3. (a) Sample preparation steps for AgNPs@Br and AgNPs@I. (b, c) Stacked SERS spectra of AgNPs@Br (orange) and AgNPs@I (red) aggregated using $MgSO_4$ or using HCl acidified $MgSO_4$ (blue). Full scale spectra (follow left *y*-axes) were displayed to show the Ag−X (X = Br, I) peaks below 300 cm^{-1}, whereas weak features are highlighted by zooming in the same spectra (indicated by the purple arrow), with *y*-axes on the right side for the scales. (d) Possible binding coordinations of AS with exposed Ag atoms on AgNPs@Br and AgNPs@I. The difference in the SERS peaks (in cm^{-1}) of AgNPs@Br/AS compared to AgNPs@I/AS is highlighted beside the associated bonds. The blue colored text highlights the partial protonation of AS and the related SERS peak.

To confirm the SERS spectra of decomposed citrate on Cl^- ligand coated AgNPs, 2 mM Na_3Cit was decomposed at 95 °C for 3 h and then added to the h-AgNPs@Cl_{part} followed by sufficient KCl and $MgSO_4$. The spectrum is a good match for AgNPs@Cl (Figure 2c, pink), with characteristic features including the 2851 and 1437 cm^{-1}, high intensity at 1399 cm^{-1} rather than at ∼1370 or ∼1410 cm^{-1}, and the absence of 1028 and 950 cm^{-1} peaks (Table S3, sample 3-8-1). According to previous studies, both citrate and ADC have SERS peaks at 950 cm^{-1} peaks, while our AAc SERS spectra feature a stronger ∼925 cm^{-1} peak and a weaker ∼890 cm^{-1} peak, indicating the absence of adsorbed citrate or ADC.[33,37]

Last but not least, when AgNPs@Cl are aggregated using HCl acidified $MgSO_4$ at a final pH = 3 ($[Cl^-]_{final}$ = 2.25 mM), the AAc^- peaks are barely identifiable, leaving ν(Ag−Cl) and water peaks as the only strong features (Figure 2c, blue). With its pK_a at 3.58, most of the AAc^- are protonated to form HAAc, therefore reducing the binding potency to Ag atoms. Also, HAAc is unstable and may readily decompose into acetone and carbon dioxide[45] accelerated by the localized heat introduced by the focused laser.

Based on the collection of evidence above, we could infer that on the AgNPs after Cl^- ligand exchange, a near-complete Cl^- layer forms on the AgNPs, and the negative charge repels citrate anions. The remaining exposed Ag atoms favor coordinate covalent bonds with the COO^- group in AAc^-. The resulting coadsorption can be described as AgNPs@Cl/AAc.

Br^- and I^- Ligand Exchanges (AgNPs@Br and AgNPs@I): The Desorption of Citrate and AAc and the Coadsorption of the Anionic Surfactant (AS) with Br^- or I^- Ligands. In the case of Br^- exchange (AgNPs@Br) followed by $MgSO_4$ aggregation (Figure 3a), the SERS spectra (Figure 3b, orange) change dramatically compared to

https://doi.org/10.1021/acs.jpcc.2c01092
J. Phys. Chem. C 2022, 126, 8692−8702

AgNPs@Cl. Prominent peaks are observed at 2926, 2896, 2845, 2723, 1590, 1461, 1440, 1302, 1128, and 720 cm^{-1}, and a characteristic peak is observed at 162 cm^{-1} (ν(Ag−Br)),[13] in addition to some vaguely resolvable peaks centered at 3067w, 1718w, and 1253w cm^{-1}. Most of these peaks are also identified upon I^- ligand exchange (AgNPs@I) and $MgSO_4$ aggregation (Figure 3c, red), with differences including the diminishing of weak features at 1253w and 1590 cm^{-1} and the rise of peaks at 1650w and 1165w cm^{-1}, as well as the advent of the distinctive peak at 110 cm^{-1} (ν(Ag−I)) in replacement of the ν(Ag−Br) peak.[15,46] Again, we confirm that the above peaks are not changed with further increases in concentrations or time allowed for ligand exchange (the maximum $[Br^-]_{final}$ or $[I^-]_{final}$ = 0.5 mM, time increases from 5 to 60 min, Figures S7 and S8). Therefore, supported by previous studies,[18,29] the strong signals could be attributed to the lack of coverage on the Ag surface by Br^- or I^- ligands, leaving gaps suitable for species to coadsorb.

To confirm the source of the peaks, Br^- and I^- ligand exchanges are also conducted on the citrate-free h-AgNPs (h-AgNPs@Br and h-AgNPs@I). The intrinsic layer of Cl^- is readily displaced by Br^- and I^-. However, in sharp contrast to h-AgNPs@Cl, the spectra of h-AgNPs@Br and h-AgNPs@I show identical strong features to the ones from citrate-reduced AgNPs (Figure S9), indicating that the species are not related to citrate or its derivatives. None of the other species that are introduced to the system such as $AgNO_3$ or NaOH (potentially contains Na_2CO_3) would provide peaks as in the spectra. The potential of bound water molecules to be the source of the above peaks is also considered. However, when the samples are prepared in the D_2O/H_2O mixture, only the bulk water peaks shift, whereas all the strong features are unchanged (Figure S10).

To identify the source of the strong features, information from previous studies was analyzed. First, similar sharp doublet peaks at 1440 and 1460 cm^{-1} are observed (but not discussed) in several studies on AgNPs or AuNPs with Br^- or I^- ligand exchanges.[13,15,17,21,47,48] It seems to indicate that this feature is not restricted to a specific experimental condition. In other words, the unknown species could be largely identical across various aqueous systems. Second, among all the studies above, only Pepera et al. showed the 2800−3000 cm^{-1} region.[20] The multiplet peaks in their KBr and KI treated AuNPs (although they cannot be deconvoluted due to low resolution) are very similar in terms of the intensity ratios compared to our AgNPs@Br and AgNPs@I. Also in the same study, their KCl treated AuNPs showed stronger peaks in the 2800−3000 cm^{-1} region, whereas adenine removed those peaks; and thus, they suggested that the unknown species are cationic and rich in carbon, oxygen, and sp^3 C−H bonds.[20] In contrast, our h-AgNPs@Cl show no peaks in 2800−3000 cm^{-1} (Figure S6, sample 3-4-1), and hence, we have to rule out cations or zwitterions.

It is also noteworthy that, when we aggregate the AgNPs@Br using HCl acidified $MgSO_4$ at a final pH = 3, no change was observed (Figure 3b); a similar result was found in AgNPs@I (Figure 3c). Hence, the species is likely to consist of functional groups that are not sensitive to pH changes to maintain its binding on the AgNPs.

As a quick summary, we found that the species could consist of the following elements:

1 universal and soluble in aqueous solutions;

2 weakly anionic or nonionic but not cationic;

3 not affected by D_2O, so no feature should be assigned to −O−H or −N−H groups;

4 only a few Raman features, so its structure should be simple or with repetitive units.

Based on these elements and the similarity to our SERS spectra, here we postulate that the species in our system is a residual anionic surfactant (AS) in a water system that contains ether groups (−C−O−C−) to support coordinative binding with Ag atoms. Polyoxyethylene alkyl ether carboxylic acid could be a suitable candidate,[49] with its general structure motif including a hydrophobic long alkyl chain, several hydrophilic ethylene oxide units, and a terminating carboxymethyl group. This type of molecule has a generic structure such as $CH_3(CH_2)_iCH_2O(CH_2CH_2O)_jCH_2COOH$ or, in short $C_iE_jCH_2COOH$, with i and j as arbitrary numbers larger than 4. Hence, the peaks on AgNPs@Br can be tentatively assigned as follows: 2926 ($\nu_s(CH_3)$), 2896 ($\nu_{as}(CH_2)$), 2845 ($\nu_s(CH_2)$), 2723 ($\tau(CH_2) + \delta(CH_2)$), 1590 ($\nu_{as}(COO^-)$, κ^2), 1461 ($\delta_s(CH_2)$, ether), 1440 ($\delta_s(CH_2)$, alkyl), 1302 ($\tau(CH_2)$), 1128 (ν(C−C)), and 720 cm^{-1} ($\rho(CH_2)$, alkyl) (Table S4, sample 4-2-2),[50−54] with its proposed binding coordinations with exposed Ag atoms depicted in Figure 3d. The different features in AgNPs@I at 1650w cm^{-1} can then be assigned to ν(C═O) in bound κ^1-COO^-, whereas the 1165w cm^{-1} peak can be related to the ν(C−O) in ether units (Table S4, sample 5-2-2).[52]

Furthermore, considering the peaks at 2925, 2891, and 2842 cm^{-1}, we found a much higher intensity ratio of 2842 cm^{-1} over the other two peaks in AgNPs@I compared to AgNPs@Br, as well as a slight blue shift in the above peaks. A similar blue shift is also observed in the doublet at 1461 and 1440 cm^{-1} (Δ = −5 cm^{-1}) (Figure S11). The shift could indicate a slightly stronger binding affinity of the species to AgNPs@I than AgNPs@Br, which is confirmed later in this study.

In summary, we propose that upon Br^- or I^- ligand exchange, the preferred adsorption of AS on the AgNPs overtakes the AAc^- probably due to its lower charge density. The COO^- and −C−O−C− groups can bind to the Ag atoms at presumed gaps in the Br^- or I^- layer. Its resistance to desorption under acidic conditions may be explained by the binding to Ag atoms via the −C−O−C− group. The resulting coadsorption can be described as AgNPs@Br/AS and AgNPs@I/AS.

An Additional Case: HS^- Ligand Exchanges (AgNPs@HS). According to the SERS intensity of the coadsorbed species on halide coated AgNPs, the sequence of surface coverage of the halide ions could be described as $Cl^- > Br^- \approx I^-$, matching a previous study based on the rate of oxidative decomposition of AgNPs.[29] However, it is worth mentioning that a much larger amount of Cl^- is required for its best coverage over the AgNPs (i.e., lowest SERS intensity from coadsorbed species) compared to Br^- or I^-. This could be explained based on the dissociation constant of Ag−X bonds: Ag−Cl > Ag−Br > Ag−I ≫ Ag−S.[55] Hence, we introduced an additional set of ligand exchange experiments using NaHS on the AgNPs. The resulting SERS spectra on AgNPs@S are very weak with only a broad feature at 225 cm^{-1} assignable to ν(Ag−S) (Figure S12),[56] suggesting that no species is coadsorbed with the HS^- layer on the AgNPs. It may be explained in a combination of two aspects: (1) the smaller radius of HS^- than I^-, leading to better coverage of small gaps,

https://doi.org/10.1021/acs.jpcc.2c01092
J. Phys. Chem. C 2022, 126, 8692−8702

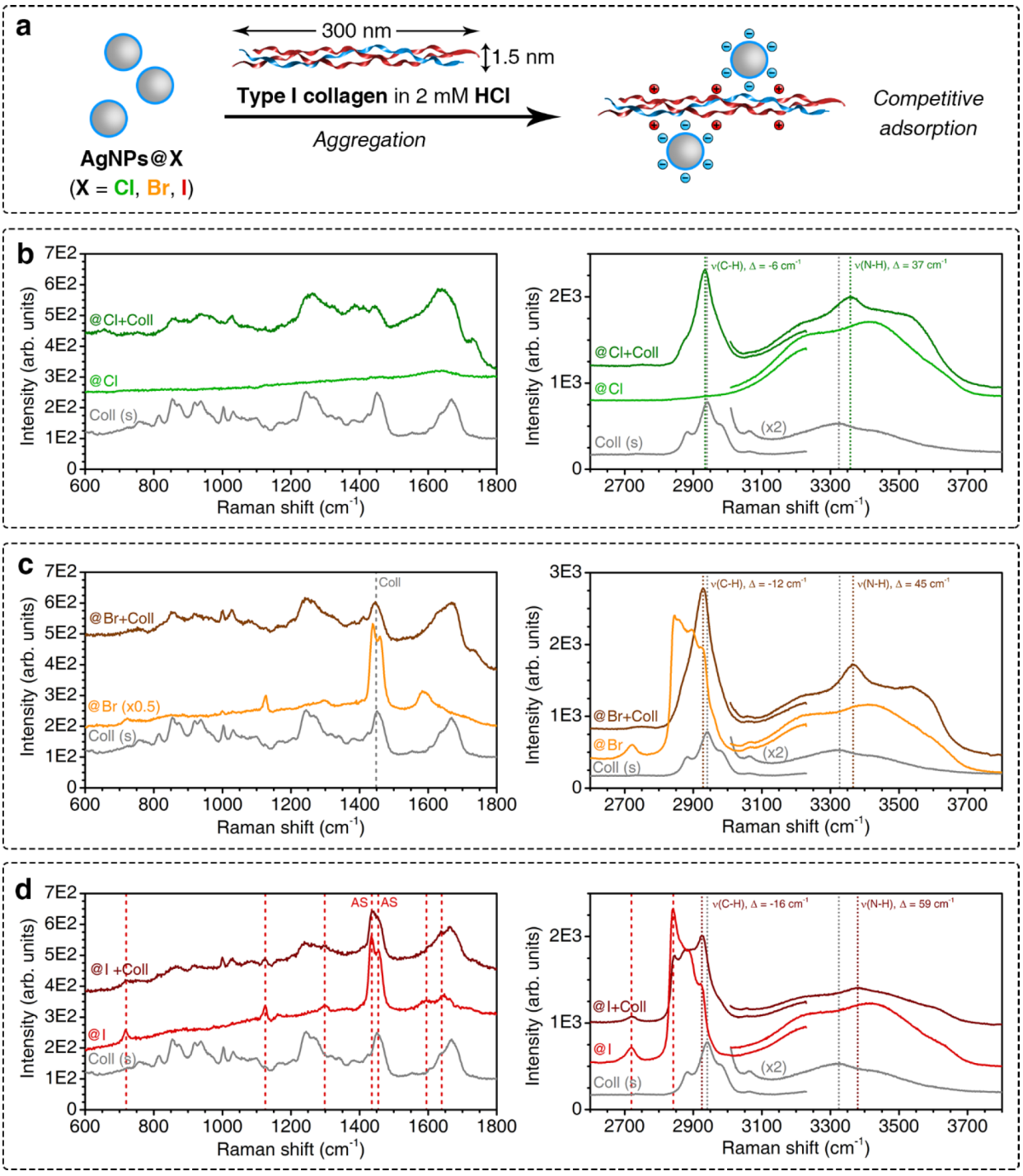

Figure 4. (a) The aggregation of AgNPs using a type I collagen solution in HCl. (b–d) Stacked SERS spectra comparing solid collagen in Raman and collagen in SERS ($[Coll]_{final}$ = 25 μg/mL) on AgNPs@X (X = Cl, Br, I).

and (2) stronger binding with Ag atoms, so as to outperform most of the organic species in our system; a study on thiol coated AuNPs also suggested a complete removal of citrate from the surface.[20] We may accordingly expand the surface coverage estimation as (Cl^-, HS^-) > (Br^-, I^-).

Binding Affinity of AS Compared to Type I Collagen: The Determinative Role of Halides. To further investigate the role of halide ligands on determining the binding affinity of coadsorbed species, a more complex system involving a bulky cationic protein was investigated.

A type I collagen solution is mixed with the AgNPs@X at a final pH = 3 (Figure 4a), to mimic a bioanalytical scenario. Since type I collagen molecules are positively charged at pH = 3,[57,58] they can be attracted to the negatively charged AgNPs@X and trigger the aggregation to ensure sufficient SERS enhancement. The aggregation of AgNPs@X with collagen would follow a similar mechanism as a previously reported nanoparticle/protein system, AuNPs@Cit/Hb (Hb = hemoglobin).[59] Therefore, when the mixing volumes are controlled, the resulting size of the aggregates is dependent on the concentration ratio [Coll]/[AgNP] in the final mixture. We

https://doi.org/10.1021/acs.jpcc.2c01092
J. Phys. Chem. C 2022, 126, 8692–8702

intentionally chose six concentrations with each two representing one aggregation mechanism to include all possible states (Figure S13). Specifically, at low collagen concentrations (0.5 to 1 μg/mL), each collagen molecule is surrounded by the maximum number of AgNPs allowed, named as "maximum coating", while excess AgNPs float around to contribute to the charge repulsion and the colloidal stability. The formation of unstable clusters is also confirmed when we increase the concentration of collagen (2.5 to 5 μg/mL), and such phenomenon is referred to as "infinite clustering". Lastly, at high collagen concentrations (10 to 25 μg/mL), "self-terminated aggregation" will occur to form finite-sized clusters with the size of the clusters determined by the adsorption kinetics, as proposed by Moerz et al.[59]

When AgNPs@Cl are mixed with collagen, no residual SERS peaks from citrate or AAc are found (Figure 4b, dark green), matching the spectrum of $MgSO_4$/HCl aggregated AgNPs@Cl. The observed SERS peaks are assignable to collagen based on a dry collagen spectrum (Table S5). SERS peaks of collagen are observed at $[Coll]_{final}$ = 25 μg/mL at 3357, 2934 ($\nu(CH_3)$; $\nu(CH_2)$), 2877 ($\nu_s(CH_3)$), 1731 (ν(C═O), in COOH of Asp or Glu), 1670 (Amide I (ν(C═O), β-sheet); $\nu_{as}(COO^-)$), 1636 (Amide I (ν(C═O), 3_{10}-helix); $\nu_{as}(COO^-)$), 1444 ($\delta(CH_3)$; $\delta(CH_2)$), 1410 ($\nu_s(COO^-)$), 1384 ($\nu_s(COO^-)$),1321 ($\tau(CH_3)$; $\tau(CH_2)$), 1264 (Amide III, δ(N−H)), 1244 (Amide III, ν(C−N)), 1027 (ν_{18a}, Phe or Tyr), 934 (ν(C−C), backbone), and 854 cm^{-1} (ν(C−C), Pro ring) (Table S5).[60−64] The enhanced $\nu_s(COO^-)$ peak at 1410 cm^{-1} could indicate the formation of direct coordinative binding of collagen with Ag atoms.

However, when AgNPs@Br are mixed with collagen, dramatic changes are observed in the SERS spectra compared to the $MgSO_4$/HCl aggregated AgNPs@Br (Figure 4c). We observe a significant decrease in the AS peaks at 2844, 2721, 1587, 1460, 1439, and 1126 cm^{-1} concurrently with the presence of strong collagen peaks. On the other hand, when mixing AgNPs@I with collagen, the AS peaks are untouched (see the red dashed lines in Figure 4d), highlighted by the strong C−H peaks at 2844 and 1438 cm^{-1} even after mixing with collagen at the highest concentration. The SERS spectra at all collagen concentrations show a clear superposition of AS and collagen features in AgNPs@I/Coll (Figure S14e and Figure S14f). Also, a much weaker peak at 1410 cm^{-1} was observed to show a diminishing direct binding of collagen to the Ag atoms.

A common peak at ∼3360 cm^{-1} that appears with all three AgNPs@X/Coll is assigned to ν_s(N−H) in NH_2 or NH_3^+ groups, with its charge driven adsorption onto the AgNPs being viewed as the cause for the blue shift to 3360 cm^{-1} from 3320 cm^{-1} in non-SERS conditions.[65] Further analysis of the ν(N−H) peak and the ν(C−H) peak (2940 cm^{-1}) from the non-SERS spectrum of collagen shows monotonic increases in the blue shifts (see the dotted lines and labels in Figures 4b, 4c, and 4d) which may indicate the strongest electrostatic interaction of the NH_3^+ group to the I^- ligand layer, followed by Br^- and Cl^-.

The functional groups in collagen that can be identified in the SERS spectra are important for elucidating the competitive adsorption with AS on the AgNPs (Figure S15). The $-COO^-/-COOH$ groups in collagen are apt to form coordinate bonds with Ag atoms, whereas the $-NH_x^+$ (x = 1, 2, 3) groups can electrostatically attach to the negatively charged surface of AgNPs@X. These groups are present at the terminals of collagen molecules but are more abundant in side chains[66] such as Lys and Arg (for $-NH_x^+$) and the shorter Asp and Glu (for $-COO^-$), which are exposed on the surface of proteins in general.[67] The −C−OH group in much shorter side chains like Ser or Hyp may also assist binding with Ag atoms as supportive electron donors.

In the case of AS, it shares similar Ag−O binding mechanisms via $-COO^-/-COOH$ and −C−O−C− groups yet lacks the electrostatic attraction via the $-NH_x^+$ groups. Since the property of the molecule supports an affinity of AS < Coll, the overall AS > Coll could then be related to the property of AgNPs@I. While the spectrum suggests a stronger collagen binding via the NH_3^+ group as the ligands change from Cl^- to Br^- and then to I^-, the other collagen peaks showed no significant shifts but a weakening binding via the $-COO^-$ group. In contrast, the above-mentioned blue shift of the C−H peak of AS coadsorbed on AgNPs@I shows stronger direct coordinative binding with Ag atoms. We can speculate that a strong "shielding effect" due to the increasing radius of halide ions (Cl^- < Br^- < I^-) supports the higher binding affinity of AS than collagen.

Now, based on the above discussions and evidence, we are able to elucidate the binding in the coadsorbing layer, which can be more accurately described as AgNPs@[(A/B)/C], with A representing the strong ligands (that dominate the binding with Ag atoms), B also directly binding with Ag atoms but filling the presumed gaps of A, and C weakly attaching to AgNPs indirectly over the layer of A and B through electrostatic interactions. With Br^- ligands, the adsorption of collagen causes AS to desorb from the AgNPs, forming AgNPs@[(Br/gap)/Coll]. With I^- ligands, AS are "shielded" by the "deeper" gaps by I^- ions due to its largest radius among the three. The exposed Ag sites would be hardly accessible by collagen side chains, and the resulting coadsorption can be described as AgNPs@[(I/AS)/Coll]. The coadsorption mechanism may also be applicable to other proteins with adequate amounts of $-COO^-$, $-NH_3^+$, and −C−OH groups in the amino acid side chains.[68]

CONCLUSION

Based on our SERS study, we demonstrated the variations in the coadsorption affinity of citrate, AAc, and AS with different halide ligands on AgNPs (in Table 1).

Table 1. Summary of the Coadsorption Conditions and an Estimated Sequence of Their Affinity to Bind to AgNPs in the Presence of Different Halide Ligands

	affinity comparison	
ligand	neutral	acidic (collagen)
no halide	Cit > (AAc, AS)[a]	
Cl^-	Cit ≈ AS ≈ 0; AAc > 0	AAc ≈ Cit ≈ AS ≈ 0; Coll > 0
Br^-	AS > (AAc, Cit)	Coll > AS > (AAc, Cit)
I^-	AS > (AAc, Cit)	AS > Coll > (AAc, Cit)

[a]Undefined sequence in the brackets.

Without halide ligand exchange, we confirm that citrate dominates the binding to AgNPs via the COO−Ag bond, while other species (AAc or AS) are not favored to coadsorb on AgNPs@Cit as indicated by the absence of the ∼2850 cm^{-1} peak.

https://doi.org/10.1021/acs.jpcc.2c01092
J. Phys. Chem. C 2022, 126, 8692−8702

When AgNPs are coated by Cl^- ligands, citrate is no longer favored to coadsorb due to its strong negative charge. Instead, AAc can coadsorb with Cl^- onto the few exposed Ag atoms. AS is not as favored in this condition.

Unlike Cl^- (or HS^-) ligands which form compact layers on the AgNPs, bulkier Br^- or I^- ligands were confirmed to leave gaps, allowing the coadsorption with AS. In contrast, small anions (Cit or AAc) are increasingly repelled by the thicker negatively charged surface layer, giving near zero affinity. An increase in the affinity of AS could be explained by a "shielding effect" again due to the thickening of the negatively charged layer of halides from Br^- to I^-, leading to the deepening of the presumed gaps, which supports AS to prevail in the competitive coadsorption with collagen.

In addition to the main findings, it is also interesting to note that AgNPs@[(Br/gap)/Coll] spectra match the best to the solid collagen in relative peak intensities (Figure 4c) while giving the strongest −N−H peak (~3370 cm^{-1}) among the three (although not the greatest blue shift). It may be a coincidence, but the observation could also be attributed to the combination of the following aspects: (i) The weak direct binding due to the thickness of the Br^- ligand layer−The charge-transfer (CT) mechanism for SERS is known to distort the protein structure.[69] (ii) The attraction due to the $-NH_x^+$ group of which the distribution over the collagen molecule is arbitrary and, therefore, allows uniform near-field enhancement via the electromagnetic (EM) mechanism. (iii) The weaker binding affinity of AS rather than collagen as explained−It could explain the fact that Br^- is a common option for ligand exchange on AgNPs for bioanalytical applications to resolve native protein structures. However, the above discussions are preliminary and may inspire researchers to undertake further studies to elaborate and resolve them in detail.

■ ASSOCIATED CONTENT

Supporting Information

The Supporting Information is available free of charge at https://pubs.acs.org/doi/10.1021/acs.jpcc.2c01092.

TEM, SAED, and UV−vis extinction spectra of AgNPs and h-AgNPs; additional SERS/Raman spectra; details of preparation methods for all samples; and SERS/Raman peak assignments (PDF)

■ AUTHOR INFORMATION

Corresponding Author

Yi Zhang − *The MacDiarmid Institute for Advanced Materials and Nanotechnology, School of Chemical and Physical Sciences, Victoria University of Wellington, Wellington 6140, New Zealand; Leather and Shoe Research Association of New Zealand, Palmerston North 4446, New Zealand;* orcid.org/0000-0002-4196-3036; Email: ethan.zhang@lasra.co.nz

Authors

Sujay Prabakar − *Leather and Shoe Research Association of New Zealand, Palmerston North 4446, New Zealand;* orcid.org/0000-0003-4371-9085

Eric C. Le Ru − *The MacDiarmid Institute for Advanced Materials and Nanotechnology, School of Chemical and Physical Sciences, Victoria University of Wellington, Wellington 6140, New Zealand;* orcid.org/0000-0002-3052-9947

Complete contact information is available at: https://pubs.acs.org/10.1021/acs.jpcc.2c01092

Notes

The authors declare no competing financial interest.

■ ACKNOWLEDGMENTS

The authors acknowledge the Ministry of Business, Innovation and Employment of New Zealand (MBIE) for the financial support through grant LSRX-1801. The authors thank Sapar Asby for providing the collagen solution and also thank Dr. David Flynn for technical assistance for the TEM measurements.

■ REFERENCES

(1) Barber, D. J.; Freestone, I. C. An Investigation of the Origin of the Colour of the Lycurgus Cup by Analytical Transmission Electron Microscopy. *Archaeometry* **1990**, *32*, 33−45.

(2) Faraday, M. Experimental Relations of Gold (and Other Metals) to Light. *Philosophical Transactions of the Royal Society of London* **1857**, *147*, 145−181.

(3) Mie, G. Beiträge Zur Optik Trüber Medien, Speziell Kolloidaler Metallösungen. *Annalen der Physik* **1908**, *330*, 377−445.

(4) Sabela, M.; Balme, S.; Bechelany, M.; Janot, J. M.; Bisetty, K. A Review of Gold and Silver Nanoparticle-Based Colorimetric Sensing Assays. *Adv. Eng. Mater.* **2017**, *19*, 1700270.

(5) Tahir, M. A.; Dina, N. E.; Cheng, H.; Valev, V. K.; Zhang, L. Surface-Enhanced Raman Spectroscopy for Bioanalysis and Diagnosis. *Nanoscale* **2021**, *13*, 11593−11634.

(6) Lu, W.; Senapati, D.; Wang, S.; Tovmachenko, O.; Singh, A. K.; Yu, H.; Ray, P. C. Effect of Surface Coating on the Toxicity of Silver Nanomaterials on Human Skin Keratinocytes. *Chemical physics letters* **2010**, *487*, 92−96.

(7) Wei, L.; Lu, J.; Xu, H.; Patel, A.; Chen, Z.-S.; Chen, G. Silver Nanoparticles: Synthesis, Properties, and Therapeutic Applications. *Drug discovery today* **2015**, *20*, 595−601.

(8) Pradhan, N.; Pal, A.; Pal, T. Silver Nanoparticle Catalyzed Reduction of Aromatic Nitro Compounds. *Colloids Surf., A* **2002**, *196*, 247−257.

(9) Rossi, L. M.; Fiorio, J. L.; Garcia, M. A.; Ferraz, C. P. The Role and Fate of Capping Ligands in Colloidally Prepared Metal Nanoparticle Catalysts. *Dalton Transactions* **2018**, *47*, 5889−5915.

(10) Lee, P. C.; Meisel, D. Adsorption and Surface-Enhanced Raman of Dyes on Silver and Gold Sols. *J. Phys. Chem.* **1982**, *86*, 3391−3395.

(11) Nie, S.; Emory, S. R. Probing Single Molecules and Single Nanoparticles by Surface-Enhanced Raman Scattering. *Science* **1997**, *275*, 1102−1106.

(12) Bastús, N. G.; Merkoçi, F.; Piella, J.; Puntes, V. Synthesis of Highly Monodisperse Citrate-Stabilized Silver Nanoparticles of up to 200 Nm: Kinetic Control and Catalytic Properties. *Chem. Mater.* **2014**, *26*, 2836−2846.

(13) Stefancu, A.; Lee, S.; Zhu, L.; Liu, M.; Lucacel, R. C.; Cortés, E.; Leopold, N. Fermi Level Equilibration at the Metal−Molecule Interface in Plasmonic Systems. *Nano Lett.* **2021**, *21*, 6592−6599.

(14) Xu, L.-J.; Lei, Z.-C.; Li, J.; Zong, C.; Yang, C. J.; Ren, B. Label-Free Surface-Enhanced Raman Spectroscopy Detection of DNA with Single-Base Sensitivity. *J. Am. Chem. Soc.* **2015**, *137*, 5149−5154.

(15) Torres-Nuñez, A.; Faulds, K.; Graham, D.; Alvarez-Puebla, R. A.; Guerrini, L. Silver Colloids as Plasmonic Substrates for Direct Label-Free Surface-Enhanced Raman Scattering Analysis of DNA. *Analyst* **2016**, *141*, 5170−5180.

(16) Dai, X.; Fu, W.; Chi, H.; Mesias, V. S. D.; Zhu, H.; Leung, C. W.; Liu, W.; Huang, J. Optical Tweezers-Controlled Hotspot for Sensitive and Reproducible Surface-Enhanced Raman Spectroscopy Characterization of Native Protein Structures. *Nat. Commun.* **2021**, *12*, 1292.

(17) Huang, J.-Y.; Zong, C.; Xu, L.-J.; Cui, Y.; Ren, B. Clean and Modified Substrates for Direct Detection of Living Cells by Surface-Enhanced Raman Spectroscopy. *Chem. Commun.* **2011**, *47*, 5738−5740.
(18) Xie, L.; Lu, J.; Liu, T.; Chen, G.; Liu, G.; Ren, B.; Tian, Z. Key Role of Direct Adsorption on Sers Sensitivity: Synergistic Effect among Target, Aggregating Agent, and Surface with Au or Ag Colloid as Surface-Enhanced Raman Spectroscopy Substrate. *journal of physical chemistry letters* **2020**, *11*, 1022−1029.
(19) Park, J.-W.; Shumaker-Parry, J. S. Strong Resistance of Citrate Anions on Metal Nanoparticles to Desorption under Thiol Functionalization. *ACS Nano* **2015**, *9*, 1665−1682.
(20) Perera, G. S.; Athukorale, S. A.; Perez, F.; Pittman Jr, C. U.; Zhang, D. Facile Displacement of Citrate Residues from Gold Nanoparticle Surfaces. *J. Colloid Interface Sci.* **2018**, *511*, 335−343.
(21) Wang, H.; Xue, Z.; Wu, Y.; Gilmore, J.; Wang, L.; Fabris, L. Rapid Sers Quantification of Trace Fentanyl Laced in Recreational Drugs with a Portable Raman Module. *Analytical chemistry* **2021**, *93*, 9373−9382.
(22) Sarina, S.; Waclawik, E. R.; Zhu, H. Photocatalysis on Supported Gold and Silver Nanoparticles under Ultraviolet and Visible Light Irradiation. *Green Chem.* **2013**, *15*, 1814−1833.
(23) Zong, C.; Xu, M.; Xu, L. J.; Wei, T.; Ma, X.; Zheng, X. S.; Hu, R.; Ren, B. Surface-Enhanced Raman Spectroscopy for Bioanalysis: Reliability and Challenges. *Chem. Rev.* **2018**, *118*, 4946−4980.
(24) Henglein, A.; Giersig, M. Formation of Colloidal Silver Nanoparticles: Capping Action of Citrate. *J. Phys. Chem. B* **1999**, *103*, 9533−9539.
(25) Janardhanan, R.; Karuppaiah, M.; Hebalkar, N.; Rao, T. N. Synthesis and Surface Chemistry of Nano Silver Particles. *Polyhedron* **2009**, *28*, 2522−2530.
(26) Lee, K. J.; Lee, Y.-I.; Shim, I.-K.; Joung, J.; Oh, Y. S. Direct Synthesis and Bonding Origins of Monolayer-Protected Silver Nanocrystals from Silver Nitrate through in Situ Ligand Exchange. *J. Colloid Interface Sci.* **2006**, *304*, 92−97.
(27) Gan, W.; Xu, B.; Dai, H. L. Activation of Thiols at a Silver Nanoparticle Surface. *Angew. Chem., Int. Ed.* **2011**, *50*, 6622−6625.
(28) AbdulHalim, L. G.; Kothalawala, N.; Sinatra, L.; Dass, A.; Bakr, O. M. Neat and Complete: Thiolate-Ligand Exchange on a Silver Molecular Nanoparticle. *J. Am. Chem. Soc.* **2014**, *136*, 15865−15868.
(29) Espinoza, M. G.; Hinks, M. L.; Mendoza, A. M.; Pullman, D. P.; Peterson, K. I. Kinetics of Halide-Induced Decomposition and Aggregation of Silver Nanoparticles. *J. Phys. Chem. C* **2012**, *116*, 8305−8313.
(30) Stewart, A.; Zheng, S.; McCourt, M. R.; Bell, S. E. Controlling Assembly of Mixed Thiol Monolayers on Silver Nanoparticles to Tune Their Surface Properties. *ACS Nano* **2012**, *6*, 3718−3726.
(31) Bell, S. E. J.; Sirimuthu, N. M. S. Surface-Enhanced Raman Spectroscopy as a Probe of Competitive Binding by Anions to Citrate-Reduced Silver Colloids. *J. Phys. Chem. A* **2005**, *109*, 7405−7410.
(32) Wei, H.; Leng, W.; Song, J.; Liu, C.; Willner, M. R.; Huang, Q.; Zhou, W.; Vikesland, P. J. Real-Time Monitoring of Ligand Exchange Kinetics on Gold Nanoparticle Surfaces Enabled by Hot Spot-Normalized Surface-Enhanced Raman Scattering. *Environ. Sci. Technol.* **2019**, *53*, 575−585.
(33) Grys, D.-B.; de Nijs, B.; Salmon, A. R.; Huang, J.; Wang, W.; Chen, W.-H.; Scherman, O. A.; Baumberg, J. J. Citrate Coordination and Bridging of Gold Nanoparticles: The Role of Gold Adatoms in Aunp Aging. *ACS Nano* **2020**, *14*, 8689−8696.
(34) Ng, H. W.; Zhang, Y.; Naffa, R.; Prabakar, S. Monitoring the Degradation of Collagen Hydrogels by Collagenase Clostridium Histolyticum. *Gels* **2020**, *6*, 46−46.
(35) Leopold, N.; Lendl, B. A New Method for Fast Preparation of Highly Surface-Enhanced Raman Scattering (Sers) Active Silver Colloids at Room Temperature by Reduction of Silver Nitrate with Hydroxylamine Hydrochloride. *J. Phys. Chem. B* **2003**, *107*, 5723−5727.
(36) Lin, X.-M.; Cui, Y.; Xu, Y.-H.; Ren, B.; Tian, Z.-Q. Surface-Enhanced Raman Spectroscopy: Substrate-Related Issues. *Anal. Bioanal. Chem.* **2009**, *394*, 1729−1745.
(37) Munro, C.; Smith, W.; Garner, M.; Clarkson, J.; White, P. Characterization of the Surface of a Citrate-Reduced Colloid Optimized for Use as a Substrate for Surface-Enhanced Resonance Raman Scattering. *Langmuir* **1995**, *11*, 3712−3720.
(38) Bichara, L. C.; Lanús, H. E.; Ferrer, E. G.; Gramajo, M. B.; Brandán, S. A. Vibrational Study and Force Field of the Citric Acid Dimer Based on the Sqm Methodology. *Advances in Physical Chemistry* **2011**, *2011*, 1.
(39) Siiman, O.; Bumm, L.; Callaghan, R.; Blatchford, C.; Kerker, M. Surface-Enhanced Raman Scattering by Citrate on Colloidal Silver. *J. Phys. Chem.* **1983**, *87*, 1014−1023.
(40) Bellamy, L. J. Carboxylic Acids. In *The Infra-Red Spectra of Complex Molecules*; Dordrecht: Springer Netherlands, 1975; pp 183−202, DOI: 10.1007/978-94-011-6017-9_10.
(41) Kerker, M.; Siiman, O.; Bumm, L. A.; Wang, D. S. Surface Enhanced Raman Scattering (Sers) of Citrate Ion Adsorbed on Colloidal Silver. *Applied optics* **1980**, *19*, 3253−3255.
(42) Tada, H.; Bronkema, J.; Bell, A. T. Application of in Situ Surface-Enhanced Raman Spectroscopy (Sers) to the Study of Citrate Oxidation on Silica-Supported Silver Nanoparticles. *Catalysis letters* **2004**, *92*, 93−99.
(43) Park, J.-W.; Shumaker-Parry, J. S. Structural Study of Citrate Layers on Gold Nanoparticles: Role of Intermolecular Interactions in Stabilizing Nanoparticles. *J. Am. Chem. Soc.* **2014**, *136*, 1907−1921.
(44) Hasi, W.-L.-J.; Lin, X.; Lou, X.-T.; Lin, S.; Yang, F.; Lin, D.-Y.; Lu, Z.-W. Chloride Ion-Assisted Self-Assembly of Silver Nanoparticles on Filter Paper as Sers Substrate. *Appl. Phys. A: Mater. Sci. Process.* **2015**, *118*, 799−807.
(45) Hay, R.; Bond, M. Kinetics of the Decarboxylation of Acetoacetic Acid. *Aust. J. Chem.* **1967**, *20*, 1823−1828.
(46) Assis, M. d.; Groppo Filho, F. C.; Pimentel, D. S.; Gouveia, A. F.; Tassia FD, C.; Fukushima, H.; Foggi, C. C.; da Costa, J. P.; Borra, R. C.; Andres, J. Ag Nanoparticles/Agx (X= Cl, Br and I) Composites with Enhanced Photocatalytic Activity and Low Toxicological Effects. *ChemistrySelect* **2020**, *5*, 4655.
(47) Li, M. D.; Cui, Y.; Gao, M. X.; Luo, J.; Ren, B.; Tian, Z. Q. Clean Substrates Prepared by Chemical Adsorption of Iodide Followed by Electrochemical Oxidation for Surface-Enhanced Raman Spectroscopic Study of Cell Membrane. *Analytical chemistry* **2008**, *80*, 5118−5125.
(48) Dong, X.; Gu, H.; Liu, F. Study of the Surface-Enhanced Raman Spectroscopy of Residual Impurities in Hydroxylamine-Reduced Silver Colloid and the Effects of Anions on the Colloid Activity. *Spectrochimica Acta - Part A: Molecular and Biomolecular Spectroscopy* **2012**, *88*, 97−101.
(49) Chiappisi, L. Polyoxyethylene Alkyl Ether Carboxylic Acids: An Overview of a Neglected Class of Surfactants with Multiresponsive Properties. *Adv. Colloid Interface Sci.* **2017**, *250*, 79−94.
(50) Okabayashi, H.; Okuyama, M.; Kitagawa, T. The Raman Spectra of Surfactants and the Concentration Dependence of Their Molecular Conformations in Aqueous Solutions. *Bull. Chem. Soc. Jpn.* **1975**, *48*, 2264−2269.
(51) Orendorff, C. J.; Ducey, M. W., Jr; Pemberton, J. E. Quantitative Correlation of Raman Spectral Indicators in Determining Conformational Order in Alkyl Chains. *J. Phys. Chem. A* **2002**, *106*, 6991−6998.
(52) Guo, C.; Liu, H.; Wang, J.; Chen, J. Conformational Structure of Triblock Copolymers by Ft-Raman and Ftir Spectroscopy. *J. Colloid Interface Sci.* **1999**, *209*, 368−373.
(53) Holland-Moritz, K.; Hummel, D.-O. Structural Studies on Linear Aliphatic Polyesters by Electron Diffraction, Infrared, and Raman Spectroscopy. *J. Mol. Struct.* **1973**, *19*, 289−300.
(54) Czamara, K.; Majzner, K.; Pacia, M. Z.; Kochan, K.; Kaczor, A.; Baranska, M. Raman Spectroscopy of Lipids: A Review. *J. Raman Spectrosc.* **2015**, *46*, 4−20.

https://doi.org/10.1021/acs.jpcc.2c01092
J. Phys. Chem. C 2022, 126, 8692−8702

(55) Li, H.; Xia, H.; Ding, W.; Li, Y.; Shi, Q.; Wang, D.; Tao, X. Synthesis of Monodisperse, Quasi-Spherical Silver Nanoparticles with Sizes Defined by the Nature of Silver Precursors. *Langmuir* **2014**, *30*, 2498−2504.
(56) Joo, T. H.; Kim, M. S.; Kim, K. Surface-Enhanced Raman Scattering of Benzenethiol in Silver Sol. *Journal of Raman spectroscopy* **1987**, *18*, 57−60.
(57) Highberger, J. H. The Isoelectric Point of Collagen. *J. Am. Chem. Soc.* **1939**, *61*, 2302−2303.
(58) Zhang, Z.; Li, G.; Shi, B. Physicochemical Properties of Collagen, Gelatin and Collagen Hydrolysate Derived from Bovine Limed Split Wastes. *Journal of the Society of Leather Technologists and Chemists* **2006**, *90*, 23.
(59) Moerz, S. T.; Kraegeloh, A.; Chanana, M.; Kraus, T. Formation Mechanism for Stable Hybrid Clusters of Proteins and Nanoparticles. *ACS Nano* **2015**, *9*, 6696−6705.
(60) Brown, G. M.; Hope, G. A. Sers Study of the Adsorption of Gelatin at a Copper Electrode in Sulfuric Acid Solution. *J. Electroanal. Chem.* **1995**, *397*, 293−300.
(61) Gullekson, C.; Lucas, L.; Hewitt, K.; Kreplak, L. Surface-Sensitive Raman Spectroscopy of Collagen I Fibrils. *Biophysical journal* **2011**, *100*, 1837−1845.
(62) Movasaghi, Z.; Rehman, S.; Rehman, I. U. Raman Spectroscopy of Biological Tissues. *Appl. Spectrosc. Rev.* **2007**, *42*, 493−541.
(63) Zhang, Y.; Mehta, M.; Mansel, B. W.; Ng, H. W.; Liu, Y.; Holmes, G.; Le Ru, E. C.; Prabakar, S. Anion-Regulated Binding Selectivity of Cr (Iii) in Collagen. *Biopolymers* **2020**, *111*, No. e23406.
(64) Frushour, B. G.; Koenig, J. L. Raman Scattering of Collagen, Gelatin, and Elastin. *Biopolymers* **1975**, *14*, 379−391.
(65) Jastrzebska, M.; Wrzalik, R.; Kocot, A.; Zalewska-Rejdak, J.; Cwalina, B. Raman Spectroscopic Study of Glutaraldehyde-Stabilized Collagen and Pericardium Tissue. *Journal of Biomaterials Science, Polymer Edition* **2003**, *14*, 185−197.
(66) Bowes, J. H.; Elliott, R.; Moss, J. The Composition of Collagen and Acid-Soluble Collagen of Bovine Skin. *Biochem. J.* **1955**, *61*, 143−150.
(67) Rose, G. D.; Geselowitz, A. R.; Lesser, G. J.; Lee, R. H.; Zehfus, M. H. Hydrophobicity of Amino Acid Residues in Globular Proteins. *Science* **1985**, *229*, 834−838.
(68) Greenwood, N. N.; Earnshaw, A. *Chemistry of the Elements*; Elsevier: 2012.
(69) Xu, L. J.; Zong, C.; Zheng, X. S.; Hu, P.; Feng, J. M.; Ren, B. Label-Free Detection of Native Proteins by Surface-Enhanced Raman Spectroscopy Using Iodide-Modified Nanoparticles. *Analytical chemistry* **2014**, *86*, 2238−2245.

https://doi.org/10.1021/acs.jpcc.2c01092
J. Phys. Chem. C 2022, 126, 8692−8702

Coadsorbed Species with Halide Ligands on Silver Nanoparticles with Different Binding Affinities

Yi Zhang,[*,†,‡] *Sujay Prabakar,*[‡] *Eric C. Le Ru*[†]

[†] The MacDiarmid Institute for Advanced Materials and Nanotechnology, School of Chemical and Physical Sciences, Victoria University of Wellington, P.O. Box 600, Wellington 6140, New Zealand

[‡] Leather and Shoe Research Association of New Zealand, P.O. Box 8094, Palmerston North 4446, New Zealand

*E-mail address: ethan.zhang@lasra.co.nz

Characterization and data correction methods

UV-Vis spectroscopy

UV-Vis extinction spectra of silver nanoparticles were measured using a Cloudspec spectrophotometer (Marama Labs, New Zealand)[1] covering wavelengths from 250 nm to 800 nm.

Transmission electron microscopy (TEM) and selected area electron diffraction (SAED)

TEM samples were diluted using DI water and casted onto formvar/carbon coated copper grids (200mesh, ProSciTech, Australia). Images were acquired with and JEOL 2100F electron microscope operated at 200 keV and the SAED pattern was acquired using a Gatan 833J45N camera.

Flat-field correction for the SERS/Raman spectra

To identify and correct the artificial features on the notch filter and the uneven response of the CCD, we collected a series of spectra of a continuous white light and fitted to polynomial functions. The relative discrepancies of the spectra were: (1) averaged to identify the feature of the notch filter; (2) rearranged according to the raw pixels of the CCD and averaged to identify the uneven response of the CCD.

Preparation of silver nanoparticles

TEM, SAED, UV-Vis extinction spectra of AgNPs and h-AgNPs

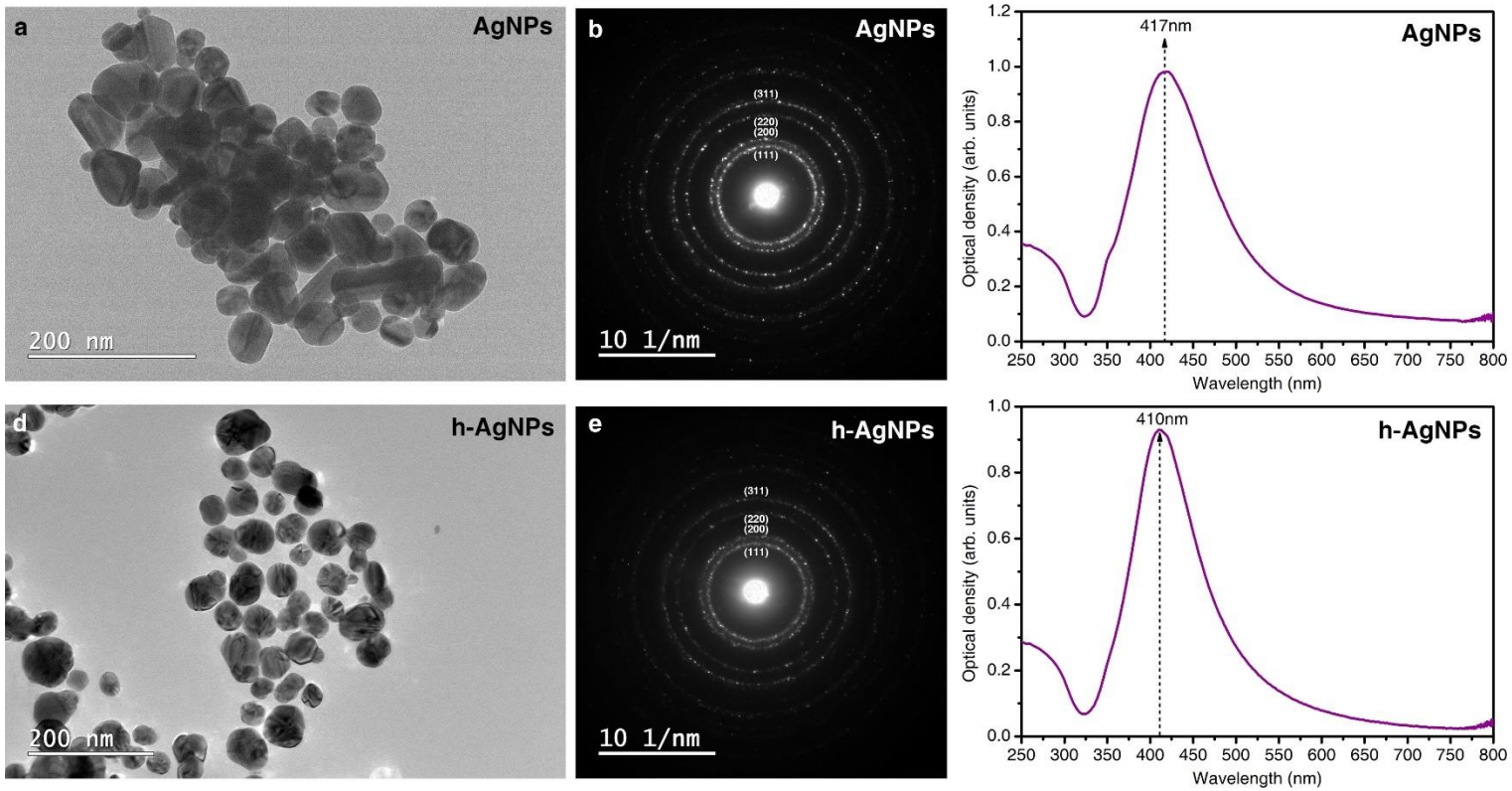

Figure S1. TEM images, SAED patterns and UV-Vis extinction spectra of AgNPs following Lee-Meisel's method[2] and h-AgNPs following Leopold's method[3]. For UV-Vis, both AgNPs and h-AgNPs were centrifuged at 5 krpm for 15 min to concentrate to 1/10 of the original volume. Dilution factor (DF) = 40.

Centrifugation speed and time of AgNPs

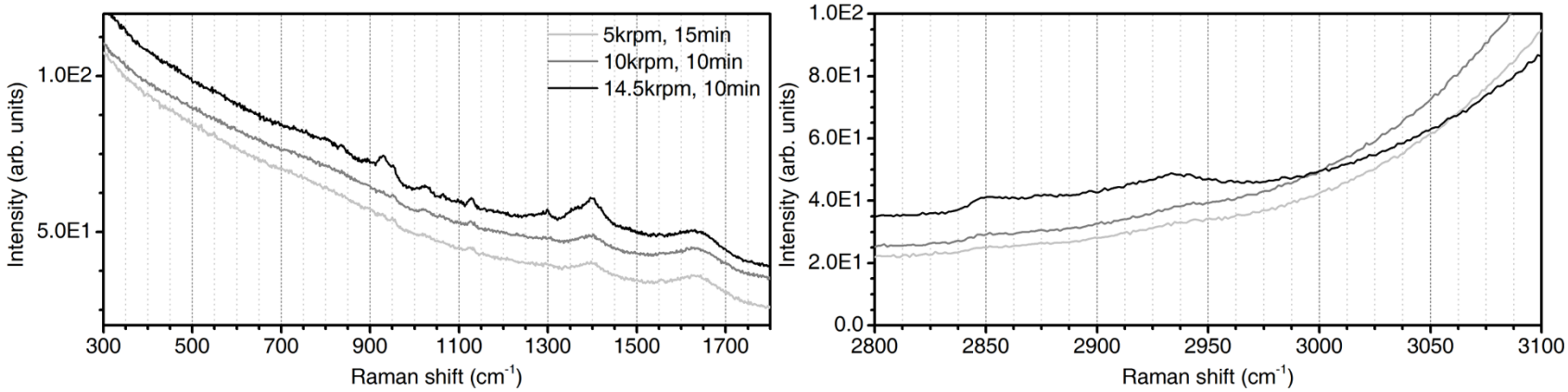

Figure S2. SERS spectra showing aggregation induced by high-speed centrifugation speed in AgNPs (sample number from bottom: 1-1-1, 1-1-2, 1-1-3).

Noticeable aggregation caused by centrifugation at 14.5 krpm is identified using SERS before adding $MgSO_4$ or protein. To avoid this, we investigate the effect of centrifugation speed and time to choose a point at which good AgNPs recovery rate is achieved with low aggregation.

Cl^- ligand exchange

Optimization of KCl concentration and time for AgNPs

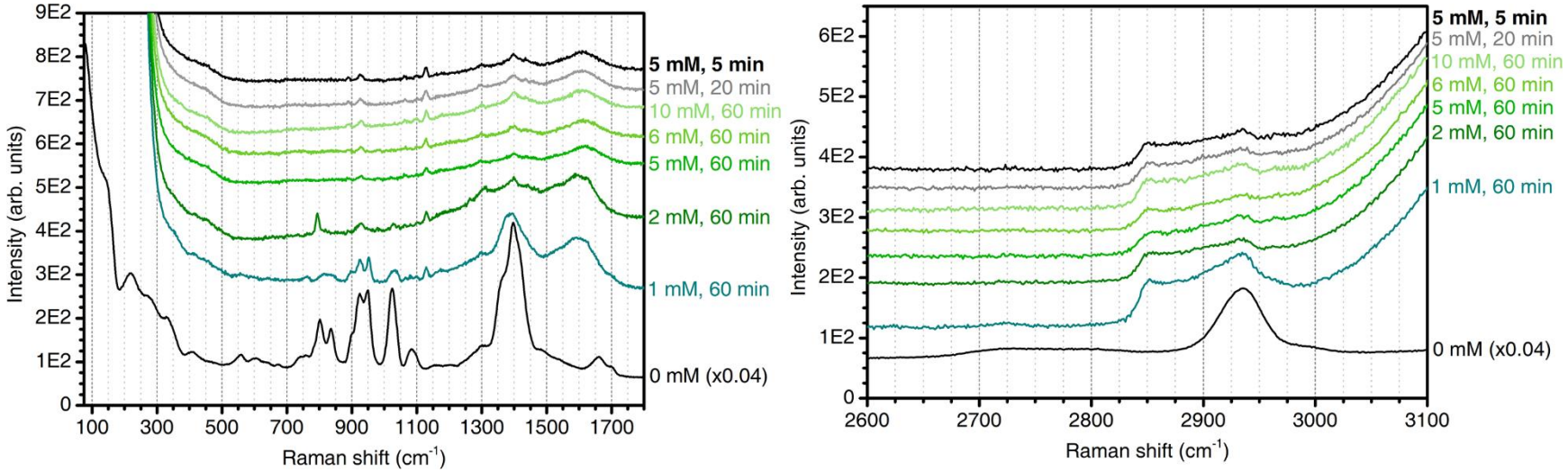

Figure S3. Stacked SERS spectra of the concentration and time series for ligand exchange of AgNPs using KCl (sample number from bottom: 2-1-1, 3-1-1, 3-1-2, 3-1-3, 3-1-4, 3-1-5, 3-2-1, 3-2-2).

Investigation of the species on AgNPs@Cl using citrate-free synthesis (h-AgNPs)

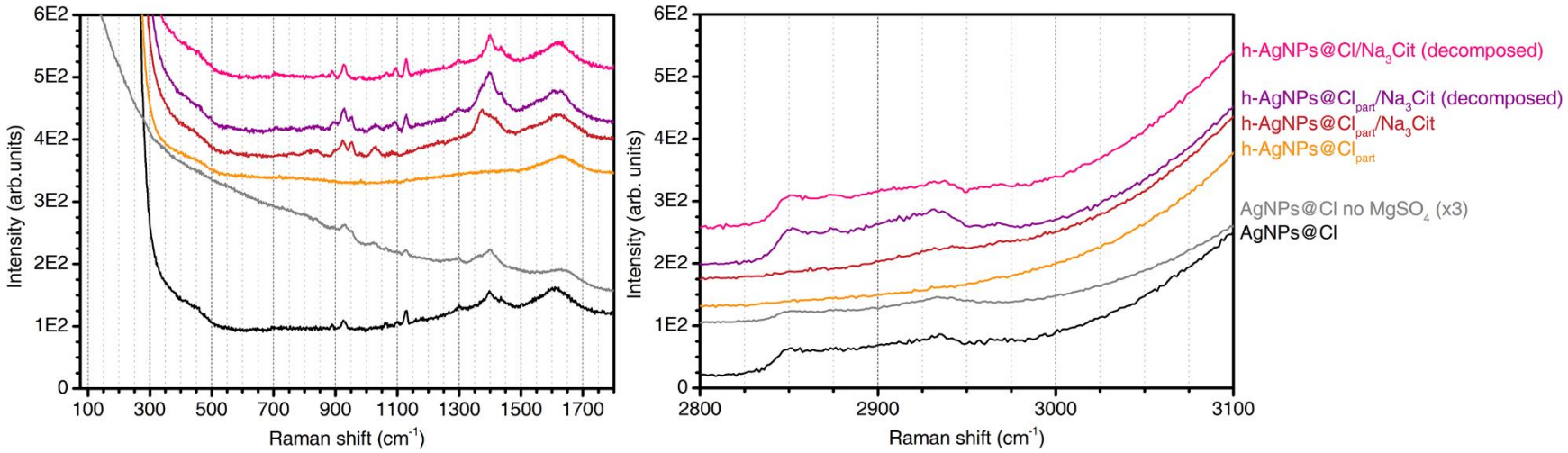

Figure S4. Stacked SERS spectra of the investigation of coadsorbed species on AgNPs@Cl (sample number from bottom: 3-1-3, 1-1-3, 3-3-1, 3-5-3, 3-6-1, 3-8-1).

With the partial coverage of Cl^- on h-AgNPs@Cl_{part}, SERS of citrate can be observed in h-AgNPs@Cl_{part}/Na_3Cit (compare sample 3-5-3 vs blank sample 3-3-1), however different from the bound species on AgNPs@Cl (which has sufficient Cl^-, sample 3-1-3). Heat decomposition at 95°C for 3 h in solution partially oxidize the citrate to acetoacetate, showing changes in the spectra to (h-AgNPs@Cl_{part}/Na_3Cit (decomposed), sample 3-6-1). Adding sufficient Cl^- in this case (h-AgNPs@Cl/Na_3Cit (decomposed), sample 3-8-1) removes the bound citrate (indicated by the 920 cm^{-1} peak and the ~1370 cm^{-1} shoulder), gives same spectra as AgNPs@Cl.

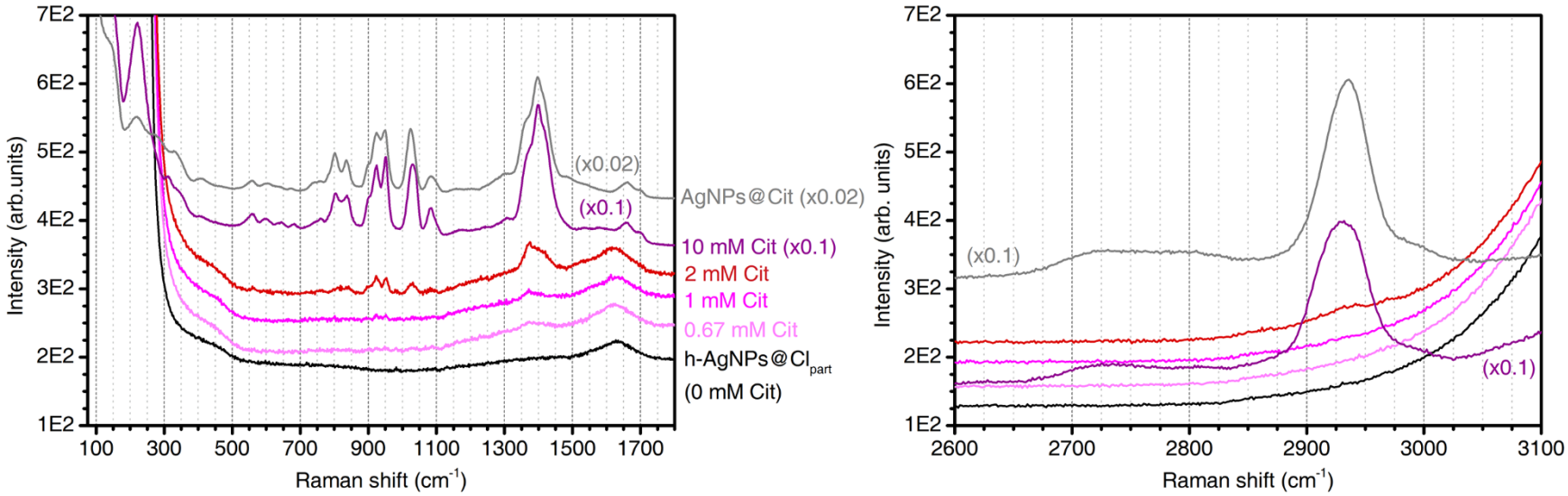

Figure S5. Stacked SERS spectra of citrate binding on h-AgNPs@Cl_{part} (sample number from bottom: 3-3-1, 3-5-1, 3-5-2, 3-5-3, 3-5-4, 2-1-1).

The intrinsic Cl^- layer on h-AgNPs@Cl_{part} is not sufficient to cover the surface, therefore we observed fresh citrate species on the SERS spectra, as the concentration goes higher ($[Cit]_{add}$ = 10 mM, so $[Cit]_{final}$ = 2.5 mM, sample 3-5-4), the spectra become similar to the as-prepared citrate-reduced AgNPs@Cit without ligand exchange (sample 2-1-1).

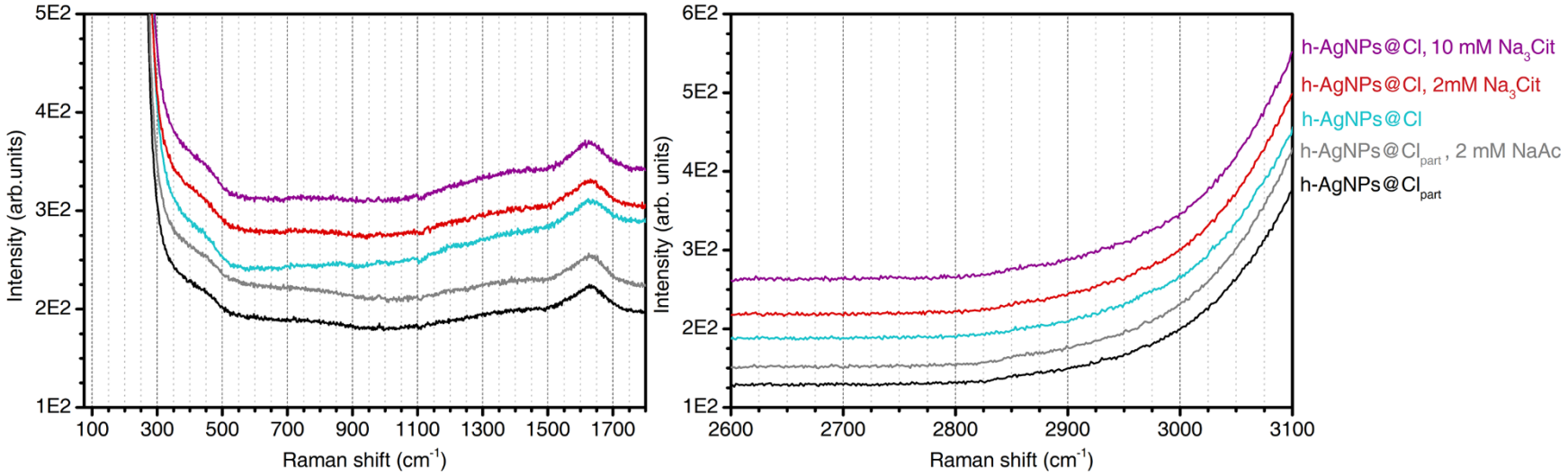

Figure S6. Stacked SERS spectra of citrate and its derivative binding on h-AgNPs@Cl (sample number from bottom: 3-4-1, 3-3-1, 3-7-1, 3-9-1, 3-9-2).

Additional experiment on sodium acetate added to h-AgNPs@Cl_{part} shows blank spectra as control. Similarly, with sufficient Cl^-, even when 10 mM Na_3Cit is added, no SERS peak from citrate molecule can be observed on h-AgNPs@Cl.

Br^- and I^- ligand exchange

Optimization of KBr concentration and time for AgNPs

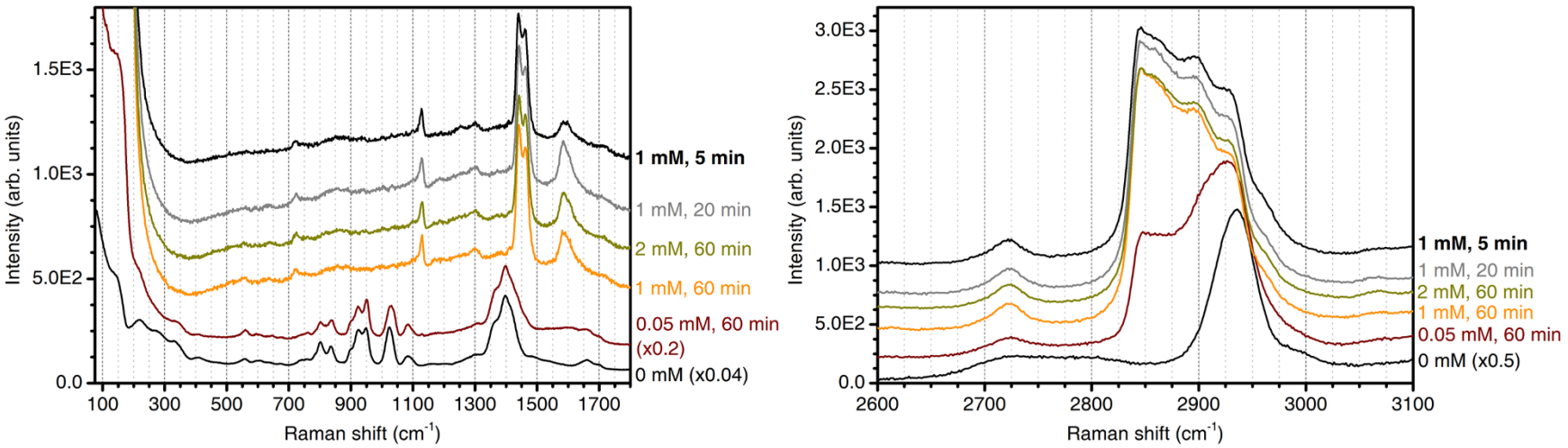

Figure S7. Stacked SERS spectra of the concentration and time series for ligand exchange of AgNPs using KBr (sample number from bottom: 2-1-1, 4-1-1, 4-1-2, 4-1-3, 4-2-1, 4-2-2).

Optimization of KI concentration and time for AgNPs

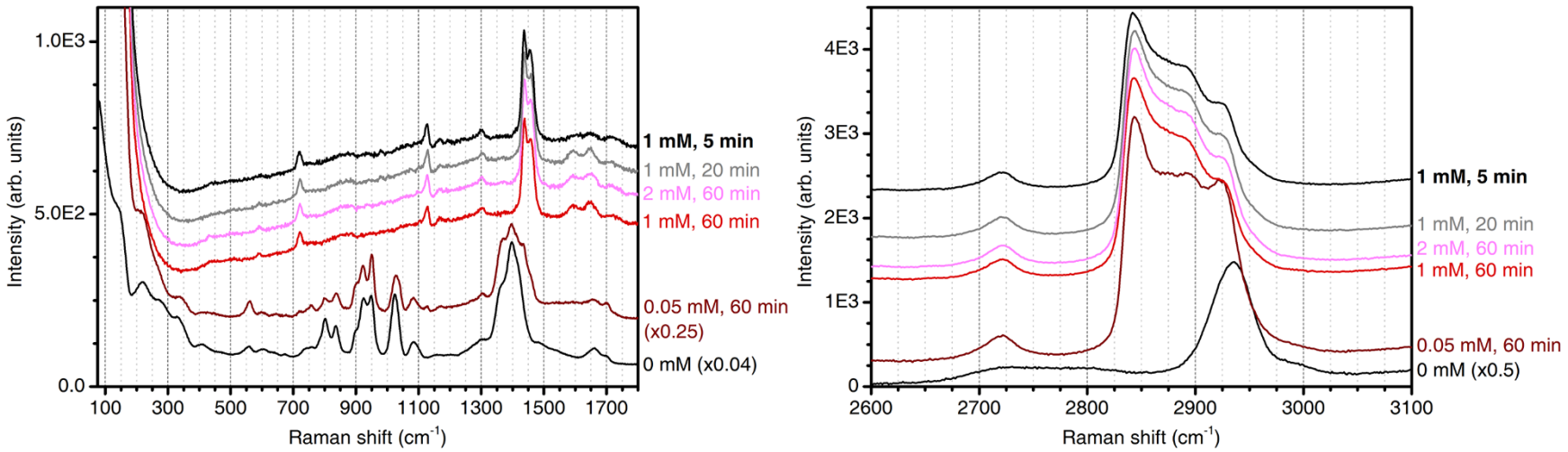

Figure S8. Stacked SERS spectra of the concentration and time series for ligand exchange of AgNPs using KI (sample number from bottom: 2-1-1, 5-1-1, 5-1-2, 5-1-3, 5-2-1, 5-2-2).

Investigation of the species on AgNPs@Br and AgNPs@I using citrate-free synthesis (h-AgNPs)

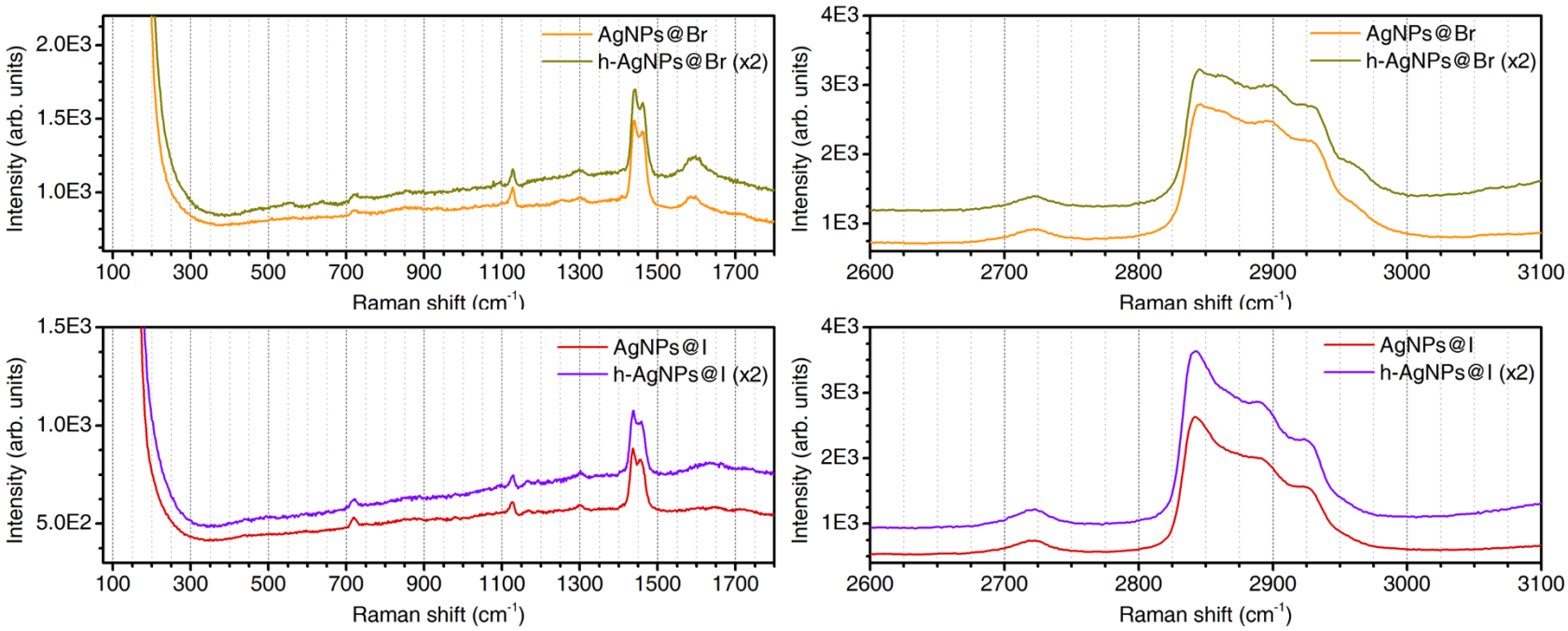

Figure S9. Stacked SERS spectra of AgNPs@X and h-AgNPs@X (X = Br, I), showing similar residual peaks with or without citrate-related species (sample number: AgNPs@Br, 4-2-2; h-AgNPs@Br, 6-1-1; AgNPs@I, 5-2-2; h-AgNPs@I, 6-2-1;).

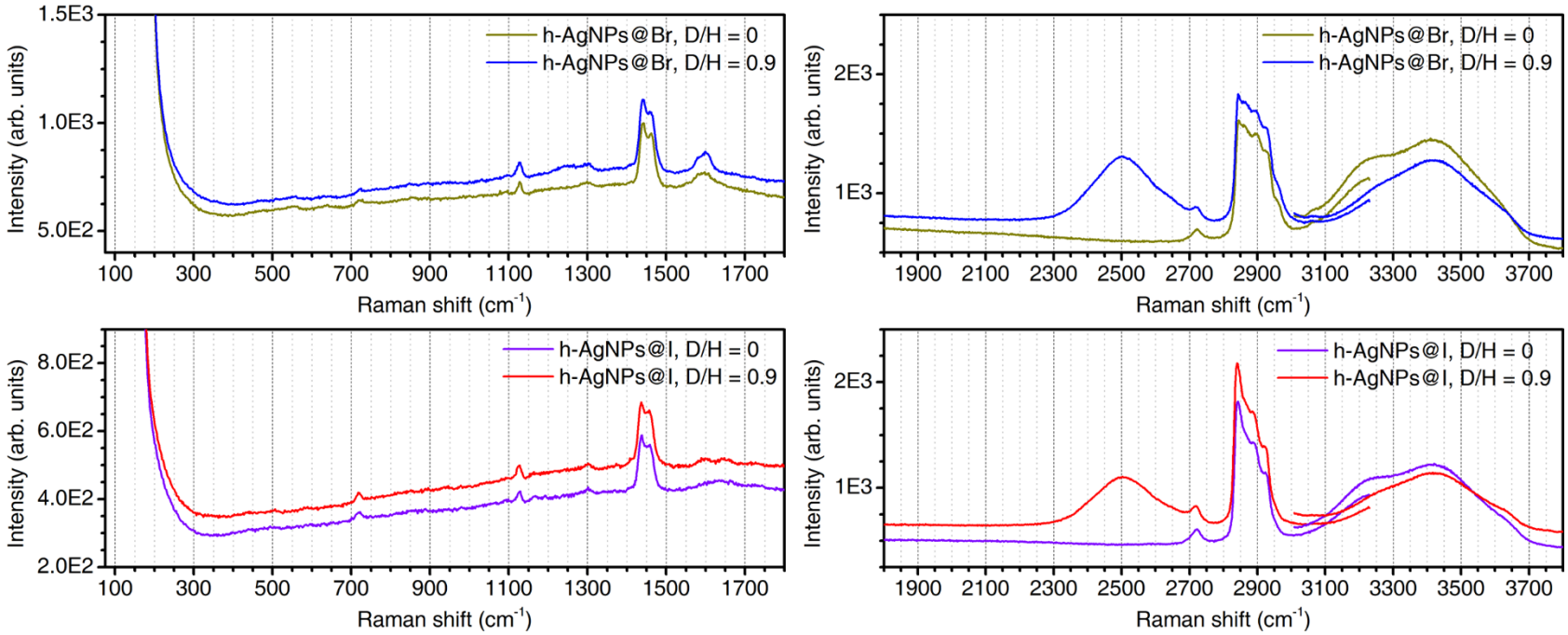

Figure S10. Stacked SERS spectra of h-AgNPs@X (X = Br, I) with D_2O exchange, showing similar residual peaks in sample in D_2O:H_2O = 190:210 ≈ 0.9 compared to pure H_2O sample (sample number: h-AgNPs@Br in H_2O, 6-1-1; h-AgNPs@Br in D_2O/H_2O, 6-3-1; h-AgNPs@I in H_2O, 6-2-1; h-AgNPs@I in D_2O/H_2O, 6-4-1;).

C−H vibrations of AS on Br^- or I^- modified surface of AgNPs

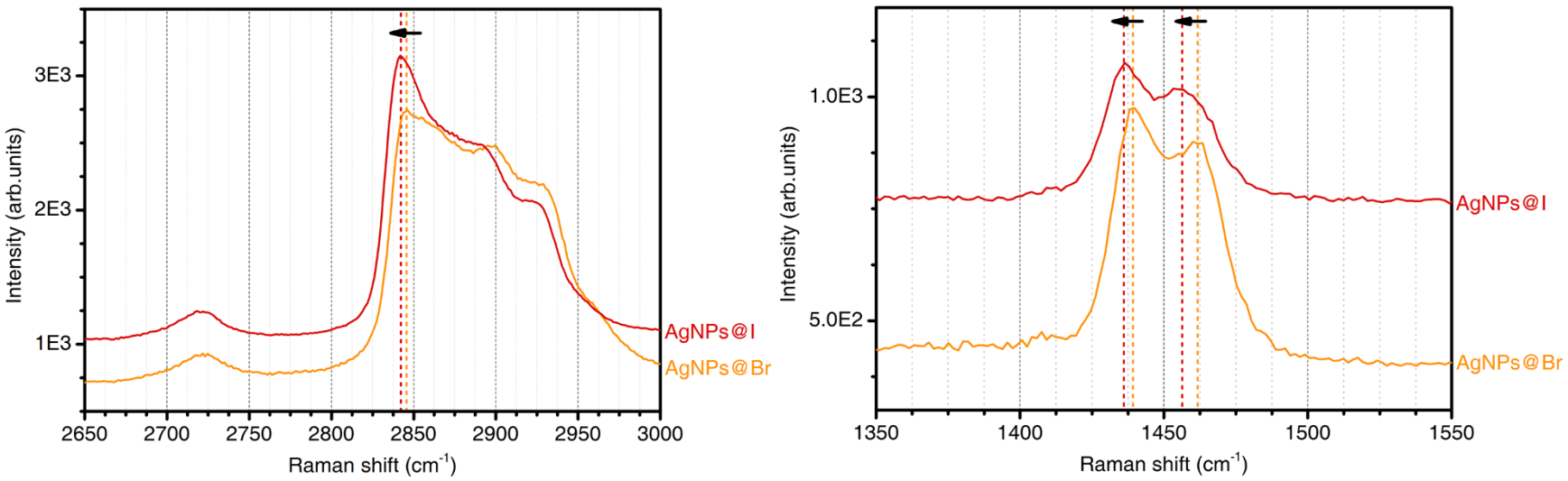

Figure S11. Stacked SERS spectra of AgNPs@X (X = Br, I) highlighting the relative changes in C−H peak intensity and the blue shifts of the peak center (sample number: AgNPs@Br, 4-2-2; AgNPs@I, 5-2-2;).

AgNPs@HS concentration series and the aggregation using collagen

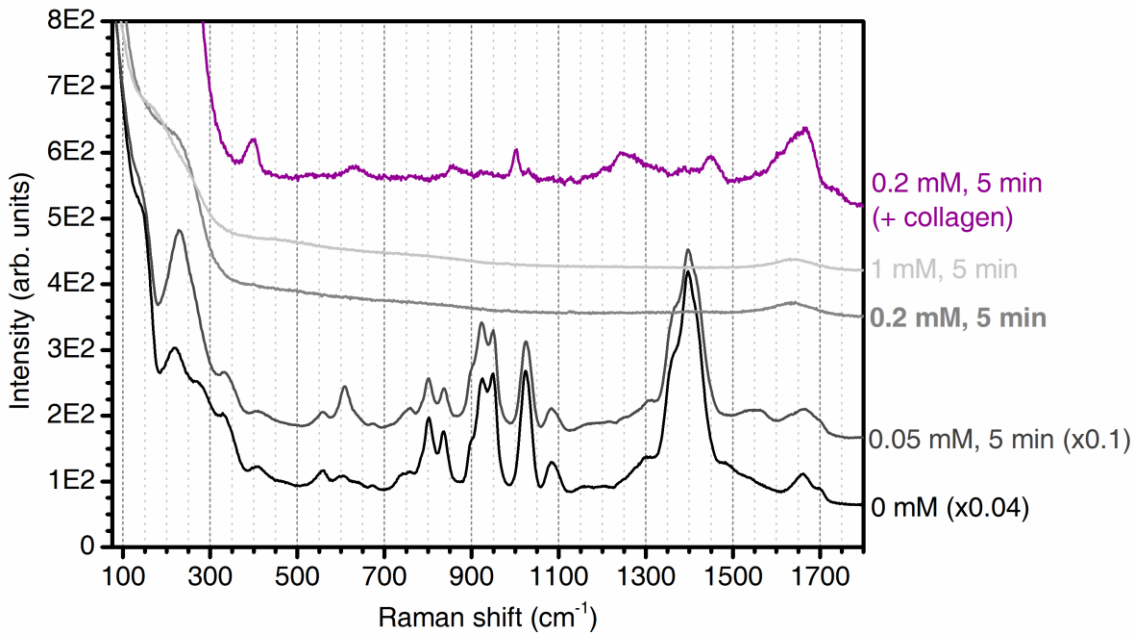

Figure S12. Stacked SERS spectra of the concentration and time series for NaHS ligand exchange for preparing AgNPs@HS, as well as a collagen spectrum on AgNPs@HS (sample number from bottom: 2-1-1, 7-1-1, 7-1-2, 7-1-3, 7-2-1).

The SERS spectrum of collagen suggests that the AgNPs is not completely etched (oxidatively decomposed) by the addition of 0.2 mM of NaHS within the time period of the SERS measurement. Therefore, the absence of coadsorbed species due to ligand exchange of HS^- is confirmed.

Investigation of the binding affinity of the coadsorbed species in competition with type I collagen

AgNPs aggregation states at different concentration ratio [Coll]/[AgNPs]

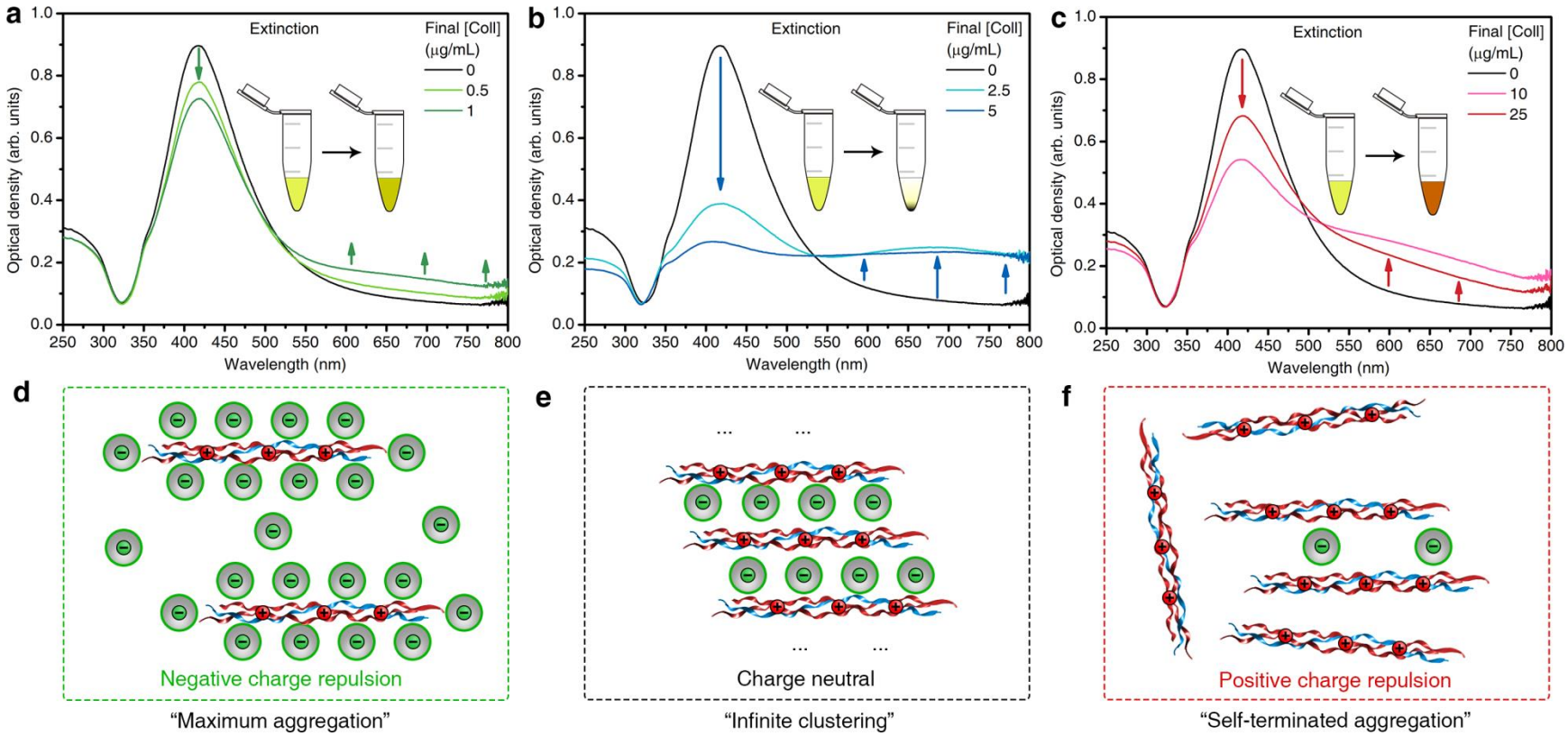

Figure S13. (a, b, c) The changes in the UV-Vis extinction spectra and the visual color changes. (d, e, f) The proposed aggregation mechanisms of AgNPs@Cl with collagen at [Coll] = 0.5 to 25 μg/mL.

SERS spectra of aggregated AgNPs@X (X = Cl, Br, I) at different collagen concentrations

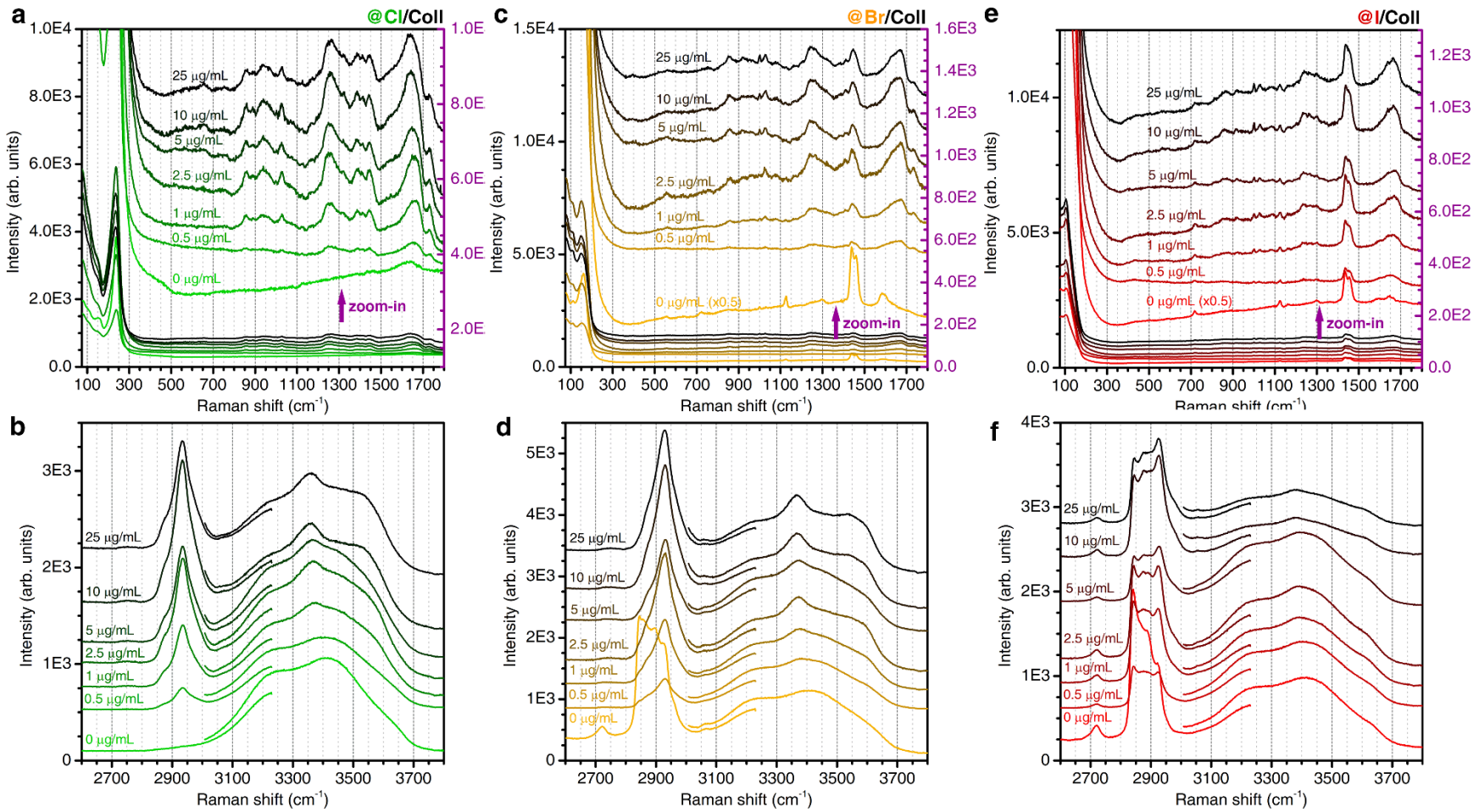

Figure S14. Stacked SERS spectra of AgNPs@X (X = Cl, Br, I) aggregated using HCl acidified $MgSO_4$ (@Cl = green, @Br = orange, @I = red) and AgNPs@X/Coll of $[Coll]_{final}$ at 0.5, 1, 2.5, 5, 10 and 25 µg/mL (as labelled).

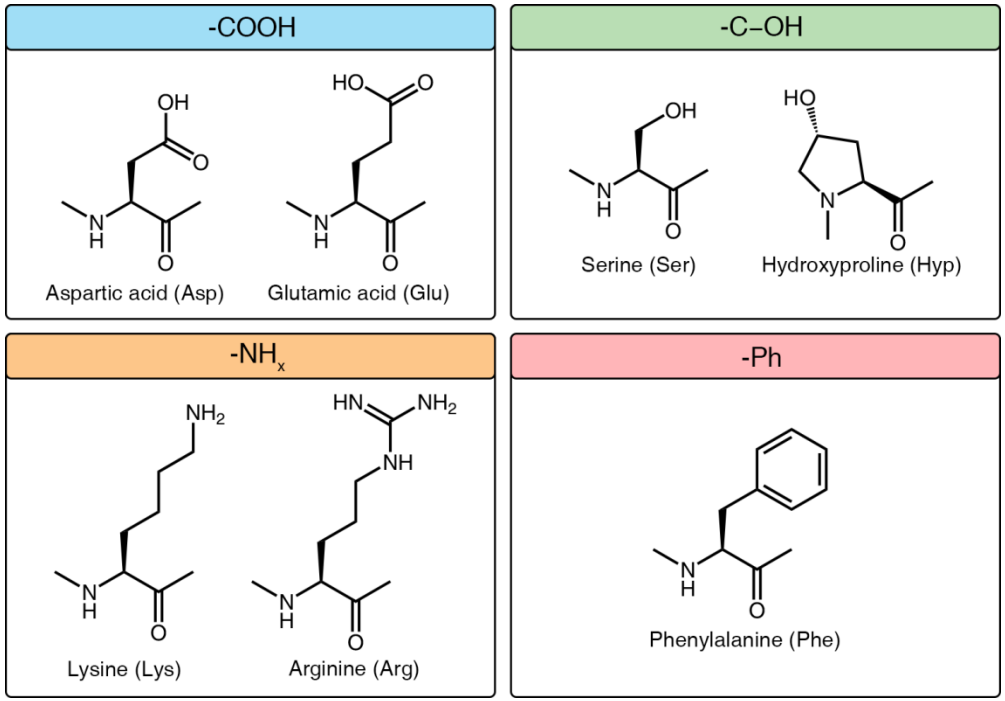

Figure S15. Amino acid residues in collagen that contain side chains functional groups that bind to AgNPs, including -COOH, -C−OH, -NH_x and -Ph (i.e., -C_6H_5).

Summary of preparation methods for all samples: centrifugation, ligand exchange and aggregation of the silver nanoparticles

Table S1. Extended sample preparation methods including the optimization of centrifugation and ligand exchange conditions. The optimized parameters are **underlined and bold**. All samples are prepared using Eppendorf Protein LoBind® 1.5mL tubes.

Experiment		**Centrifugation: rotational speed and time**	**Ligand exchange: type of salt, concentration and time**	**Aggregation: salt or collagen concentration, and acid concentration**	**Sample number (#)**
Ligand +coadsorbed species	**Volume (µL)**	1000 − 900 = 100 µL	100 + 100 (or split into specified volumes, e.g., 50 + 50) = 200 µL	200 + 200 = 400 µL	
1. Centrifugation					
Cit	**AgNPs@Cit:** Rotational speed and time	**<u>5 krpm, 15 min;</u>** 10 krpm, 10 min; 14.5 krpm, 10 min;	-	-	1-1-1 1-1-2 1-1-3
2. Citrate adsorption					
Cit	**AgNPs@Cit**	5 krpm, 15 min;	DI water, 5 min;	5 mM $MgSO_4$;	2-1-1
3. Ligand exchange: Cl^-					

Cl +AAc	**AgNPs@Cl:** KCl concentration	5 krpm, 15 min;	1 mM KCl, 60 min; 2 mM KCl, 60 min; **<u>5 mM KCl,</u>** 60 min **($[Cl^-]_{final}$ = 1.25 mM);** 6 mM KCl, 60 min; 10 mM KCl, 60 min;	5 mM $MgSO_4$;	3-1-1 3-1-2 3-1-3 3-1-4 3-1-5
Cl +AAc	**AgNPs@Cl:** KCl time	5 krpm, 15 min;	5 mM KCl, 20 min; **<u>5 mM KCl, 5 min;</u>**	5 mM $MgSO_4$;	3-2-1 3-2-2
Cl_{part}	**h-AgNPs@Cl_{part}**	5 krpm, 15 min;	DI water, 5 min;	5 mM $MgSO_4$;	3-3-1
Cl	**h-AgNPs@Cl:** KCl confirm	5 krpm, 15 min;	5 mM KCl, 5 min;	5 mM $MgSO_4$;	3-4-1
Cl_{part} +Cit	**h-AgNPs@Cl_{part}:** Add Na_3Cit	5 krpm, 15 min;	0.67 mM Na_3Cit, 5 min; 1 mM Na_3Cit, 5 min; 2 mM Na_3Cit, 5 min; 10 mM Na_3Cit, 5 min;	5 mM $MgSO_4$;	3-5-1 3-5-2 3-5-3 3-5-4
Cl_{part} +AAc	**h-AgNPs@Cl_{part}:** Add heated Na_3Cit	5 krpm, 15 min;	Heated 2 mM Na_3Cit, 5 min;	5 mM $MgSO_4$;	3-6-1

Cl_{part}	**h-AgNPs@Cl_{part}:** Add NaAc	5 krpm, 15 min;	2 mM NaAc, 5 min;	5 mM $MgSO_4$;	3-7-1
Cl +AAc	**h-AgNPs@Cl:** Extra KCl with heated Na_3Cit	5 krpm, 15 min;	65 µL of heated 2 mM Na_3Cit and 35 µL of 10 mM KCl, 5 min;	5 mM $MgSO_4$;	3-8-1
Cl	**h-AgNPs@Cl:** Extra KCl with Na_3Cit	5 krpm, 15 min;	65 µL of 2 mM Na_3Cit and 35 µL of 10 mM KCl, 5 min; 50 µL of 10 mM Na_3Cit and 50 µL of 7 mM KCl, 5 min;	5 mM $MgSO_4$;	3-9-1 3-9-2
Cl	**AgNPs@Cl:** Acidification	5 krpm, 15 min;	5 mM KCl, 5 min;	5 mM $MgSO_4$ in 2 mM HCl;	3-10-1
4. Ligand exchange: Br^-					
Br +AS	**AgNPs@Br:** KBr concentration	5 krpm, 15 min;	0.05 mM KBr, 60 min; **<u>1 mM KBr,</u>** 60 min **($[Br^-]_{final}$ = 0.25 mM);** 2 mM KBr, 60 min;	5 mM $MgSO_4$;	4-1-1 4-1-2 4-1-3
Br +AS	**AgNPs@Br:** KBr time	5 krpm, 15 min;	1 mM KBr, 20 min; **<u>1 mM KBr, 5 min;</u>**	5 mM $MgSO_4$;	4-2-1 4-2-2

Br +AS	**AgNPs@Br:** Acidification	5 krpm, 15 min;	1 mM KBr, 5 min;	5 mM $MgSO_4$ in 2 mM HCl;	4-3-1
5. Ligand exchange: I^-					
I +AS	**AgNPs@I:** KI concentrations	5 krpm, 15 min;	0.05 mM KI, 60 min; **<u>1 mM KI,</u>** 60 min; **($[I^-]_{final}$ = 0.25 mM);** 2 mM KI, 60 min;	5 mM $MgSO_4$;	5-1-1 5-1-2 5-1-3
I +AS	**AgNPs@I:** KI times	5 krpm, 15 min;	1 mM KI, 20 min; **<u>1 mM KI, 5 min;</u>**	5 mM $MgSO_4$;	5-2-1 5-2-2
I +AS	**AgNPs@I:** Acidification	5 krpm, 15 min;	1 mM KI, 5 min;	5 mM $MgSO_4$ in 2 mM HCl;	5-3-1
6. Identification of the unknown species					
Br	**h-AgNPs@Br:** KBr confirm	5 krpm, 15 min;	1 mM KBr, 5 min;	5 mM $MgSO_4$;	6-1-1
I	**h-AgNPs@I:** KI confirm	5 krpm, 15 min;	1 mM KI, 5 min;	5 mM $MgSO_4$;	6-2-1
Br	**h-AgNPs@Br:** D_2O exchange	5 krpm, 15 min;	1 mM KBr (in 90 µL D_2O and 10 µL H_2O), 5 min;	5 mM $MgSO_4$ (in 100 µL D_2O and 100 µL H_2O);	6-3-1

I	**h-AgNPs@I:** D_2O exchange	5 krpm, 15 min;	1 mM KI (in 90 µL D_2O and 10 µL H_2O), 5 min;	5 mM $MgSO_4$ (in 100 µL D_2O and 100 µL H_2O);	6-4-1
7. Additional ligand exchange: HS^-					
S	**AgNPs@HS:** NaHS concentrations	5 krpm, 15 min;	0.05 mM NaHS, 5 min; **<u>0.2 mM NaHS, 5 min</u>** **($[S^-]_{final}$ = 0.05 mM);** 1 mM NaHS, 5 min;	5 mM $MgSO_4$;	7-1-1 7-1-2 7-1-3
S +Coll	**AgNPs@HS:** Collagen aggregation	5 krpm, 15 min;	0.2 mM NaHS, 5 min;	50 µg/mL collagen in 2 mM HCl;	7-2-1
8. Aggregation using protein					
Cl +Coll, Br +Coll, I +AS +Coll	**AgNPs@Cl,** **AgNPs@Br,** **AgNPs@I:** Collagen concentrations	5 krpm, 15 min;	5 mM KCl, 5 min; 1 mM KBr, 5 min; 1 mM KI, 5 min;	0 µg/mL collagen in 2 mM HCl; 1 µg/mL collagen in 2 mM HCl; 2 µg/mL collagen in 2 mM HCl; 5 µg/mL collagen in 2 mM HCl; 10 µg/mL collagen in 2 mM HCl; 20 µg/mL collagen in 2 mM HCl; 50 µg/mL collagen in 2 mM HCl;	-

SERS/Raman data analysis

Table S2. SERS peak assignments of (1) AgNPs@Cit + $MgSO_4$, (2) h-AgNPs@Cl_{part} + Na_3Cit + $MgSO_4$. Tentative assignments by the authors are highlighted in blue color with an asterisk symbol (*).

Raman shift (cm^{-1})		**Assignment**	**Reference (cm^{-1})**
AgNPs@Cit **+ $MgSO_4$** **pH = 8**	**h-AgNPs@Cl_{part}** **+ Na_3Cit** **+ $MgSO_4$** **pH = 8** **$[Cl^-]_{final}$ = 0.375 mM** **$[Cit]_{final}$ = 0.5 mM**	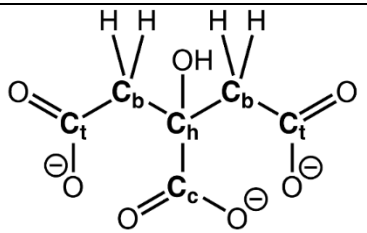 Cit^{3-}	
2-1-1	3-5-3		
3424	3414	ν_{as}(O−H), water, hydrogen bonded; [4] DA-OH, water;[5]	3435; [4] 3432;[5]
3217sh	3236sh	ν_s(O−H), water, hydrogen bonded; [4] DDAA-OH, water;[5]	3247; [4] 3226;[5]
2997sh		$\nu_{as}(CH_2)$; [6]	3000(DFT); [6]
2934	2937w	ν_s(C−H), in Cu_2(cit)·$2H_2O$; [7] $\nu_s(CH_2)$; [6]	2929; [7] 2934(DFT); [6]

2804sh			
2723		ν(O–H), in bonded -COOH; [8]	2500-2700; [8]
1700sh		$\nu(C_t–OH)$, κ^1-C_tOOH; [9]	1710; [9]
1660		$\nu(C_t=O)$, κ^1-C_tOO^-; [9]	1685; [9]
	1622	$\nu_{as}(COO^-)$; [10]	1624; [10]
1540sh		$\nu_{as}(COO^-)$; [7] $\nu_{as}(COO^-)$; [11] $\nu_{as}(C_tOO^-)$, κ^2; [9]	1555; [7] 1550; [11] 1535; [9]
1490w			
1414sh	1415sh	$\nu_s(COO^-)$; [10] $\nu_s(COO^-)$, bound; [7] $\nu_s(COO^-)$, unbound; [12] $\nu_s(COO^-)$, cit(aq); [12] $\nu_s(COO^-)$, cit(aq); [9]	1415; [10] 1415; [7] 1412; [12] 1417; [12] 1410; [9]
1397		$\nu_s(COO^-)$; [10] $\nu_s(COO^-)$; [11] $\nu_s(COO^-)$, bound; [12] $\nu_s(COO^-)$, κ^2; [9] *$\nu_s(C_cOO^-)$, bound;	1400; [10] 1392; [11] 1400; [12] 1385; [9]

1360sh	1373	$\nu_s(COO^-)$, bound; [12] $\nu_s(COO^-)$; [10] *$\nu_s(C_tOO^-)$, bound;	1370; [12] 1345; [10]
1297w		$\nu(C_t{-}O)$, κ^1 in -C_tOO^- or in -C_tOOH; [9]	1300; [9]
1084	1082vw	$\nu(C_b{-}C_h)$, c_2t_2 or c_2t_2-t_2; [9]	1080; [9]
1024	1028	$\nu_s(C{-}C)$; [10] $\nu(C{-}O)$; [12] $\nu(C_c{-}C_h)$, c_2; [9] $\nu(C_c{-}C_h)$, linked to κ^2-$C_cOO{-}Au$; [9]	1026; [10] 1025; [12] 1030(DFT); [9] 1020; [9]
948	951	$\nu(C{-}C)$; [10] $\nu(C{-}C)$, cit(aq); [11] $\nu(C{-}COO)$; [12] $\nu(C_t{-}C_b)$, unbound; [9]	956; [10] 957; [11] 952; [12] 950; [9]
925	923	$\nu(C{-}C)$, bound; [10] $\nu(C{-}C)$; [11] $\nu(C{-}COO)$; [12] *$\nu(C_t{-}C_b)$, bound;	940; [10] 933; [11] 933; [12]
899sh	899sh	$\nu(C{-}COO)$; [12]	903; [12]

835	833w	ν(C_h–O); [10] ν(C_h–O), cit(aq); [11]	845; [10] 846; [11]
801			
757w		ν(C_t–C_b), cit(aq); [9]	750; [9]
736sh			
673		δ(OCO); [7] δ(COO); [12]	680; [7] 670; [12]
641w			
602w		δ(COO); [12]	596; [12]
557		π(COO); [7] δ(COO); [12]	568; [7] 560; [12]
472w	445sh	ρ(COO); [7] ν(Ag–O), subsurface; [11]	475; [7] 464; [11]
408		ρ(COO); [13]	
332		ν(Ag–O), adsorbed; [11] Eclipsing of -C_cOO^- with -C_tOO^-; [12]	320; [11] 336; [12]
278sh			

	240	ν(Ag−Cl); [14] ν(Ag−Cl); [15] ν(Ag−Cl); [16]	245; [14] 243; [15] 240; [16]
218		ν(COO−Ag); [12]	232; [12]
147sh	158sh	Ag lattice vibration; [17]	147; [17]

Table S3. SERS peak assignments of (1) AgNPs@Cl + $MgSO_4$, (2) h-AgNPs@Cl + heat decomposed Na_3Cit + $MgSO_4$, (3) AgNPs@Cl + $MgSO_4$ in 2 mM HCl. Tentative assignments by the authors are highlighted in blue color with an asterisk symbol (*).

Raman shift (cm^{-1})			**Assignment**	**Reference (cm^{-1})**
AgNPs@Cl + $MgSO_4$ pH = 8 [Cl^-] = 1.25 mM	**h-AgNPs@Cl + heat decomposed Na_3Cit + $MgSO_4$ pH = 8 [Cl^-] = 1.25 mM [$Cit]_{eq,\ final}$ = 0.325 mM**	**AgNPs@Cl + $MgSO_4$ in 2 mM HCl pH = 3 [Cl^-] = 2.25 mM**	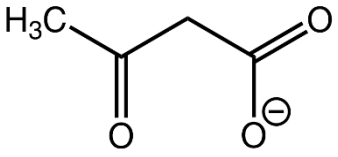 AAc^-, keto form 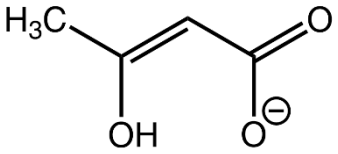 AAc^-, enol form	
3-1-3	3-8-1	3-10-1		
3624sh	3619sh	3627sh	ν_s(O−H), water, unbound; [4] Free OH, water;[5]	3627; [4] 3636;[5]
3418	3415	3418	ν_{as}(O−H), water, hydrogen bonded; [4] DA-OH, water;[5]	3435; [4] 3432;[5]
3228sh	3235sh	3228sh	ν_s(O−H), water, hydrogen bonded; [4] DDAA-OH, water;[5]	3247; [4] 3226;[5]
2967vw	2968vw		$\nu_{as}(CH_3)$, methyl acetoacetate; [18]	2962; [18]

2935	2935	2940vw	$\nu_{as}(CH_2)$, methyl acetoacetate; [18] $\nu_s(CH_2)$, methyl acetoacetate; [18]	2942; [18] 2930; [18]
2849	2851	2856vw	$\nu_s(CH_3)$, methyl acetoacetate; [18]	2849; [18]
		1640	δ(HOH), water; [19]	1641; [19]
1610	1620		ν(O–C=C), enol form, methyl acetoacetate; [18]	1627; [18]
		1450vw	*$\delta(CH_2)$, anionic surfactant (AS);	
1436sh	1437		n.a., acetoacetic acid,;[12] $\delta_s(CH_3)$, methyl acetoacetate; [18]	1442; [12] 1453; [18]
1398w	1399		n.a., acetoacetic acid; [12] *$\nu_s(COO^-)$;	1400; [12]
1299w	1299		n.a., lithium acetoacetate; [20] ω(CH_2), methyl acetoacetate; [18]	1283; [20] 1317; [18]
1128	1127		ν(CCC), methyl acetoacetate; [18] n.a., lithium acetoacetate; [20]	1158; [18] 1158; [20]
1098vw	1095		n.a., acetoacetic acid; [12] n.a., lithium acetoacetate; [20]	1085; [12] 1087; [20]
1062w	1064w			

926w	927		n.a., acetoacetic acid; [12] n.a., lithium acetoacetate; [20] ν(C−CH_3), methyl acetoacetate; [18]	935; [12] 928; [20] 903; [18]
889w	889w		n.a., lithium acetoacetate; [20] δ(CCO), methyl acetoacetate; [18]	903; [20] 875; [18]
434sh	448sh		ν(Ag−O), subsurface; [11]	464; [11]
239	240	237	ν(Ag−Cl); [14] ν(Ag−Cl); [15] ν(Ag−Cl); [16]	245; [14] 243; [15] 240; [16]
155sh	160sh	155sh	Ag lattice vibration; [17]	147; [17]

Table S4. SERS peak assignments of (1) AgNPs@Br + $MgSO_4$, (2) AgNPs@Br + $MgSO_4$ in 2 mM HCl, (3) AgNPs@I + $MgSO_4$, (4) AgNPs@I + $MgSO_4$ in 2 mM HCl. Tentative assignments by the authors are highlighted in blue color with an asterisk symbol (*).

Raman shift (cm^{-1})				**Assignment**	**Reference(cm^{-1})**
AgNPs@Br + $MgSO_4$ pH = 8	**AgNPs@Br + $MgSO_4$ in 2 mM HCl pH = 3**	**AgNPs@I + $MgSO_4$ pH = 8**	**AgNPs@I + $MgSO_4$ in 2 mM HCl pH = 3**	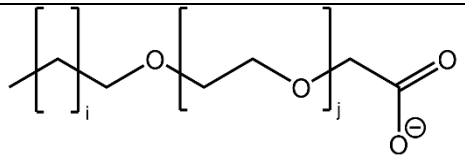 alkyl chain + ethylene oxide units + carboxylate group	
4-2-2	4-3-1	5-2-2	5-3-1		
3612sh	3618sh	3622sh	3622sh	ν_s(O−H), water, unbound; [4] Free OH, water;[5]	3627; [4] 3636;[5]
3416	3412	3420	3421	ν_{as}(O−H), water, hydrogen bonded; [4] DA-OH, water;[5]	3435; [4] 3432;[5]
3221sh	3219sh	3222sh	3219sh	ν_s(O−H), water, hydrogen bonded; [4] DDAA-OH, water;[5]	3247; [4] 3226;[5]
3067w	3064w				
2960sh	2960sh			$\nu_{as}(CH_3)$, polyethylene (PE); [21] $\nu_{as}(CH_3)$, PPO; [22] $\nu_{as}(CH_3)$, triacylglycerols; [23]	2960-2965; [21] 2970; [22] 2957-2965; [23]

2926	2924	2925sh	2921sh	$\nu_s(CH_2)_{FR}$, PE; [21] $\nu_s(CH_3)$, PPO; [22] $\nu_s(CH_3)$, fatty acids; [23]	2925; [21] 2930; [22] 2909-2937; [23]
2896	2895	2891sh	2886sh	$\nu_{as}(CH_2)$, PE; [21] $\nu_{as}(CH_2)$, PEO; [22] $\nu_{as}(CH_2)$, fatty acids; [23]	2881-2886; [21] 2880; [22] 2870-2895; [23]
2861sh	2860sh			$\nu_s(CH_2)$, fatty acids; [23]	2852-2862; [23]
2845	2844	2842	2841	$\nu_s(CH_2)$, PE; [21] $\nu_s(CH_2)$, PEO; [22] $\nu_s(CH_2)$, fatty acids; [23]	2847-2852; [21] 2850; [22] 2832-2845; [23]
2723	2721	2720	2719	*Combination mode of ($\tau(CH_2)$ + $\delta(CH_2)$);	*1300 + 1440 = 2740;
1718w	1714vw	1718vw	1722vw	ν(C=O), COOH, triacylglycerols; [23] *ν(C−OH), COOH;	1727-1730; [23]
		1650w	1646	ν(C=C), unsaturated fatty acid; [23] *ν(C=O), κ^1-COO^-;	1653-1672; [23]
1590	1587	1596w	1591sh	$\nu_{as}(COO^-)$, potassium n-alkyl carboxylate; [24] *$\nu_{as}(COO^-)$, κ^2;	1580-1600; [24]

1461	1460	1455	1456	$\delta_s(CH_2)$, potassium n-alkyl carboxylate; [24] $\delta_{as}(CH_3)$, PE; [21] $\delta_s(CH_2)$, (polyethylene oxide) PEO; [22] $\delta(CH_2)$, $\delta(CH_3)$, fatty acids; [23]	1450-1465; [24] 1445-1450; [21] 1470; [22] 1457-1464; [23]
1440	1439	1436	1434	$\delta(CH_2)$, PE; [21] $\delta_s(CH_2)$, PEO; [22] $\delta_s(CH_2)$, fatty acids; [23]	1440-1441; [21] 1448; [22] 1433-1445; [23]
1302	1299	1300	1299	$\nu(CH_2{-}CH_2)$, potassium n-alkyl carboxylate; [24] $\tau(CH_2)$, PE; [21] $\tau(CH_2)$, fatty acids; [23]	1290-1300; [24] 1295-1302; [21] 1294-1306; [23]
1253w	1251w			$\tau(CH_2)$, PEO; [22] $\delta(=C{-}H)$, fatty acid; [23]	1232; [22] 1260-1265; [23]
		1166w	1165w	$\nu(C{-}O)$, PEO; [22] $\nu(C{-}C)$, fatty acid; [23]	1141; [22] 1166-1179; [23]
1128	1126	1125	1124	$\nu(C{-}C)_T$, PE; [21] $\nu(C{-}C)$, $\omega(CH_2)$, PEO; [22] $\nu(C{-}C)$, fatty acid; [23]	1124-1128; [21] 1125; [22] 1118-1133; [23]
	1000vw				
720	720	719	719	$\rho(CH_2)$, aliphatic polyester; [25]	720; [25]

563vw	559w			δ(OCC), PEO; [22]	536; [22]
162	160			ν(Ag−Br); [17] ν(Ag−Br); [15] ν(Ag−Br); [16]	175; [17] 162; [15] 166; [16]
111w	111w				
		110	106	ν(Ag−I), A_1 transition in β-AgI polymorph; [17] ν(Ag−I); [15] ν(Ag−I); [16]	103; [17] 118; [15] 127; [16]

Table S5. SERS peaks from AgNPs@X/Coll (X = Cl, Br, I) at final collagen concentrations of 1 µg/mL and 25 µg/mL, compared to dry collagen Raman peaks with corresponding assignments. Tentative assignments by the authors are highlighted in blue color with an asterisk symbol (*). Peaks that are potentially originated from AS are **underlined and bold**.

Raman shift (cm^{-1})							**Assignment**	**Reference (cm^{-1})**
AgNPs@Cl + Coll in 2 mM HCl pH = 3		**AgNPs@Br + Coll in 2 mM HCl pH = 3**		**AgNPs@I + Coll in 2 mM HCl pH = 3**		**Dry collagen**		
1 µg/mL	**25 µg/mL**	**1 µg/mL**	**25 µg/mL**	**1 µg/mL**	**25 µg/mL**	-		
		3580sh	3580sh	3589sh	3595sh		ν_s(O−H), water, unbound; [4] ν_{as}(O−H), water, unbound; [4]	3627; [4] 3531; [4]
3556sh	3529sh		3534				*ν_{as}(N−H), bound to NPs;	
3447sh		3455sh		3454sh	3458sh	3438sh	ν_{as}(O−H), water, hydrogen bonded; [4]	3435; [4]
3367	3357	3374	3365	3390	3379		*ν_s(N−H), bound to NPs;	

						3320	ν(N−H), in amide bond or side chains; [26] ν(N−H); [27] ν(N−H), amide; [28]	3324; [26] 3300; [27] 3329; [28]
3220sh	3228sh	3222sh	3221sh	3228sh	3236sh		ν_s(O−H), water, hydrogen bonded; [4]	3247; [4]
		3063vw	3059w		3054w	3063	*ν(O−H), in hydrogen bonded -COOH in collagen;	
					2974sh	2980sh	$\nu_{as}(CH_3)$; [27]	2977; [27]
2934	2934	2930	2928	2923	2924	2940	$\nu(CH_3)$; $\nu(CH_2)$; [29] $\nu(CH_2)$; [27]	2928-2938; [29] 2937; [27]
				2892sh			**$\nu_{as}(CH_2)$, AS;**	
2876sh	2877sh	2868sh	2870sh	2874	2875	2882	$\nu_s(CH_3)$; [27]	2880; [27]
				2843	**2844**		**$\nu_s(CH_2)$, AS;**	
		2736w		**2721**	**2722**		ν(O−H), in bonded –COOH; [8] **$\tau(CH_2) + \delta(CH_2)$, AS;**	2500-2700; [8]
1732	1731	1736	1734	1730vw			ν(C=O), in -COOH of Asp or Glu in collagen; [30]	1700-1750; [30]

1660	1670sh	1673	1670	1662	1664	1666	Amide I; [31] $\nu_{as}(COO^-)$ or Amide I (β-sheet); [29]	1670 [31] 1675; [29]
1630sh	1636	1626sh	1632sh	1636sh	1638sh	1637sh	Amide I; [31] $\nu_{as}(COO^-)$ or Amide I (3_{10}-helix); [29]	1642; [31] 1632; [29]
				1594sh		1605sh	$\nu_{as}(COO^-)$ or ν_{8a}** (Phe or Tyr); [29] δ(N−H); [27]	1605; [29] 1594; [27]
						1554w	Amide II; [29] $\nu_{as}(COO^-)$; [32]	1565; [29] 1560 [32]
						1464sh	$\delta(CH_3)$; $\delta(CH_2)$; [31]	1464; [31]
				1456	**1457sh**		**$\delta(CH_2)$, AS;**	
1445	1444	1444	1446			1453	$\delta(CH_3)$; $\delta(CH_2)$; [31] C−H; ν_{19b}, Phe; [29]	1451; [31] 1445; [29]
				1435	**1438**		**$\delta(CH_2)$, AS;**	
1413	1410	1410w	1410	1406vw		1424sh	$\nu_s(COO^-)$; [31] δ(COH); [32]	1422; [31] 1424; [32]
1386	1384	1382vw	1380w			1380	$\nu_s(COO^-)$; [32] $\delta_s(CH_2)$; [26]	1389; [32] 1391; [26]

						1340w	$\omega(CH_3)$; $\omega(CH_2)$; [31] $\delta_s(CH_2)$; [26]	1343; [31] 1340; [26]
1323w	1321w	1324sh	1320sh			1318w	$\tau(CH_3)$; $\tau(CH_2)$; [31]	1314; [31]
				1300w	**1301w**		**$\tau(CH_2)$, AS;**	
1263	1264	1265	1263	1269w	1268	1270	Amide III ; [31] Amide III; C−H; ν_3, Phe; ν_3, Tyr ; [29] δ(N−H), Amide III; [26]	1271; [31] 1265-1285; [29] 1269; [26]
1242	1244	1238	1241	1240w	1239	1245	Amide III; [31] Amide III; Tyr; [29] ν(C−N), Amide III; [26] Amide III; [27]	1248; [31] 1235-1245; [29] 1251; [26] 1234-1252; [27]
		1206sh	1199sh		1204sh	1205w	Hyp; Tyr; [31] Phe; Tyr; [29]	1211; [31] 1215; [29]
	1169vw	1166vw	1162vw	1162w	1167vw	1172w	Tyr; [31] ν_{9a}, Phe; [29] $\delta(NH^+)$, Pro; [33]	1178; [31] 1175-1195; [29] 1174; [33]

1124vw		1126vw	1128vw	**1124**	**1123**	1126w	$\delta(NH_3^+)$; [33] **ν(C−C), $\omega(CH_2)$, AS;**	1136-1143; [33]
						1100	ν_{as}(COC); [26]	1094; [26]
		1079vw	1082vw	1084vw		1062vw	ν_{18b}, Phe; [29]	1065; [29]
1027	1026	1027	1028	1028	1028	1031	*ν(C−C), Pro; [31] ν_{18a}, Phe; ν_{18a}, Tyr; [29] Phe; [27]	1037; [31] 1025; [29] 1032; [27]
		1001	1001	1000	1001	1003	Phe; [31] ν_{12}, Phe; [29] ν(C−C), Phe ring; [26] Phe; [27]	1006; [31] 995; [29] 1001; [26] 1004; [27]
	966sh	966vw	966vw			969sh	Amide III'; [31]	966; [31]
940w	934					939	ν(C−C), backbone; [31] ν(C−COO^-); ν_{17a}, Phe; ν_{17a}, Tyr; [29] ν(C−C), α-helix; [26]	938; [31] 940-945; [29] 934; [26]
						920	ν(C−C), Pro ring; [31] ν(C−C); [27]	921; [31] 923; [27]
892w								

				875vw	874w	875	ν(C−C), Hyp ring; [31]	876; [31]
856	854	858w	855	855vw	854sh	855	ν(C−C), Pro ring; [31] ν_s(COC); [26] Tyr; [27]	856; [31] 862; [26] 857; [27]
					815vw	815	ν(C−C), backbone; [31] δ(CCN); δ(COC); [26]	821; [31] 810; [26]
						757w		
				718	**719w**		**ρ(CH_2), AS;**	
	658w						ω(COO^-); ν_{6b}, Tyr; [29]	645-665; [29]
		559w	560vw			566w		
						531w		
				433		424sh		
			395vw			392w		
						301w		
238	235						ν(Ag−Cl); [14] ν(Ag−Cl); [15] ν(Ag−Cl); [16]	245; [14] 243; [15] 240; [16]

		153	149				ν(Ag−Br); [17] ν(Ag−Br); [15] ν(Ag−Br); [16]	175; [17] 162; [15] 166; [16]
153sh	152sh						Ag lattice vibration; [17]	147; [17]
		111w	109w					
				104	104		ν(Ag−I), A_1 transition in β-AgI polymorph; [17] ν(Ag−I); [15] ν(Ag−I); [16]	103; [17] 118; [15] 127; [16]

Table Notations

Vibrational modes:

n.a. = not assigned by the reference; FR = Fermi resonance; G = gauche conformation; T = trans conformation;

ν, stretching; δ, bending (undefined); δ_s, in-plane scissoring; ρ, in-plane rocking; ω, out-of-plane wagging; τ, out-of-plane twisting.

Peaks shape and intensity:

w, weak (when peak maximum is easily identifiable, but too weak to have a well-defined shape);

vw, very weak (when peak center is hardly identifiable, usually assigned based on the difference or similarity with control samples);

sh, shoulder (when the proposed peak center is covered by an adjacent peak).

Citrate binding coordination on metal surface (κ^n, c_n, t_n):

n, denticity; κ, non-bridging ligand (binding to multiple metal atoms through non-continuous atoms);

c, bound via central carboxyl;[9] t, bound via terminal carboxyl;[9]

Carbon atoms (C_x):

x = c for the carbon atom in the central carboxyl group,

x = t for the carbon atom in the terminal carboxyl group;

x = h for the carbon atom linked to the hydroxyl group;

x = b for the carbon in the middle of the branch;

Asterisks:

**: Wilson notation for modes of benzene ring vibration.[34]

Amino acid residues:

Phe = phenylalanine; Tyr = Tyrosine; Pro = proline; Hyp = hydroxyproline; Asp = aspartic acid; Glu = glutamic acid; Lys = lysine; Arg = arginine; His = histidine;

The -COO^-/-COOH groups in collagen are in Asp and Glu residues (major) and on the C-terminal of the polypeptide chains (very minor);

The N−H bonds that are not part of the backbone amide bonds can be found in Arg and Lys residues (major), His residue (minor) and the N-terminal of the polypeptide chains (very minor).

References

1. Djorovic, A.; Oldenburg, S. J.; Grand, J.; Le Ru, E. C., Extinction-to-Absorption Ratio for Sensitive Determination of the Size and Dielectric Function of Gold Nanoparticles. *ACS nano* **2020**, *14*, 17597-17605.
2. Lee, P. C.; Meisel, D., Adsorption and Surface-Enhanced Raman of Dyes on Silver and Gold Sols. *Journal of Physical Chemistry* **1982**, *86*, 3391-3395.
3. Leopold, N.; Lendl, B., A New Method for Fast Preparation of Highly Surface-Enhanced Raman Scattering (Sers) Active Silver Colloids at Room Temperature by Reduction of Silver Nitrate with Hydroxylamine Hydrochloride. *Journal of Physical Chemistry B* **2003**, *107*, 5723-5727.
4. Walrafen, G., Raman Spectral Studies of the Effects of Temperature on Water Structure. *The Journal of Chemical Physics* **1967**, *47*, 114-126.
5. Sun, Q., The Raman Oh Stretching Bands of Liquid Water. *Vibrational Spectroscopy* **2009**, *51*, 213-217.
6. Bichara, L. C.; Lanús, H. E.; Ferrer, E. G.; Gramajo, M. B.; Brandán, S. A., Vibrational Study and Force Field of the Citric Acid Dimer Based on the Sqm Methodology. *Advances in Physical Chemistry* **2011**, *2011*.
7. Siiman, O.; Bumm, L.; Callaghan, R.; Blatchford, C.; Kerker, M., Surface-Enhanced Raman Scattering by Citrate on Colloidal Silver. *The Journal of Physical Chemistry* **1983**, *87*, 1014-1023.
8. Bellamy, L. J., Carboxylic Acids. In *The Infra-Red Spectra of Complex Molecules*, Springer Netherlands: Dordrecht, 1975; pp 183-202.
9. Grys, D.-B.; de Nijs, B.; Salmon, A. R.; Huang, J.; Wang, W.; Chen, W.-H.; Scherman, O. A.; Baumberg, J. J., Citrate Coordination and Bridging of Gold Nanoparticles: The Role of Gold Adatoms in Aunp Aging. *ACS nano* **2020**, *14*, 8689-8696.
10. Kerker, M.; Siiman, O.; Bumm, L. A.; Wang, D. S., Surface Enhanced Raman Scattering (Sers) of Citrate Ion Adsorbed on Colloidal Silver. *Applied optics* **1980**, *19*, 3253-3255.
11. Tada, H.; Bronkema, J.; Bell, A. T., Application of in Situ Surface-Enhanced Raman Spectroscopy (Sers) to the Study of Citrate Oxidation on Silica-Supported Silver Nanoparticles. *Catalysis letters* **2004**, *92*, 93-99.
12. Munro, C.; Smith, W.; Garner, M.; Clarkson, J.; White, P., Characterization of the Surface of a Citrate-Reduced Colloid Optimized for Use as a Substrate for Surface-Enhanced Resonance Raman Scattering. *Langmuir* **1995**, *11*, 3712-3720.
13. Bickley, R.; Edwards, H.; Gustar, R.; Rose, S., A Vibrational Spectroscopic Study of Nickel (Ii) Citrate Ni3 (C6h5o7) 2 and Its Aqueous Solutions. *Journal of molecular structure* **1991**, *246*, 217-228.
14. Bell, S. E. J.; Sirimuthu, N. M. S., Surface-Enhanced Raman Spectroscopy as a Probe of Competitive Binding by Anions to Citrate-Reduced Silver Colloids. *Journal of Physical Chemistry A* **2005**, *109*, 7405-7410.
15. Torres-Nuñez, A.; Faulds, K.; Graham, D.; Alvarez-Puebla, R. A.; Guerrini, L., Silver Colloids as Plasmonic Substrates for Direct Label-Free Surface-Enhanced Raman Scattering Analysis of DNA. *Analyst* **2016**, *141*, 5170-5180.

16. Stefancu, A.; Lee, S.; Zhu, L.; Liu, M.; Lucacel, R. C.; Cortés, E.; Leopold, N., Fermi Level Equilibration at the Metal–Molecule Interface in Plasmonic Systems. *Nano Letters* **2021**, *21*, 6592-6599.
17. Assis, M. d.; Groppo Filho, F. C.; Pimentel, D. S.; Gouveia, A. F.; Tassia FD, C.; Fukushima, H.; Foggi, C. C.; da Costa, J. P.; Borra, R. C.; Andres, J., Ag Nanoparticles/Agx (X= Cl, Br and I) Composites with Enhanced Photocatalytic Activity and Low Toxicological Effects. **2020**.
18. Schiavoni, M.; Di Loreto, H.; Hermann, A.; Mack, H. G.; Ulic, S.; Della Védova, C., Keto‐Enol Tautomerism in β-Ketoesters: Ch3c (O) Chxc (O) Oy (X= H, Cl; Y= Ch3, C2h5). Vibrational Analyses, Nmr Spectra and Quantum Chemical Calculations. *Journal of Raman Spectroscopy* **2001**, *32*, 319-329.
19. Carey, D. M.; Korenowski, G. M., Measurement of the Raman Spectrum of Liquid Water. *The Journal of chemical physics* **1998**, *108*, 2669-2675.
20. De Gelder, J.; De Gussem, K.; Vandenabeele, P.; Moens, L., Reference Database of Raman Spectra of Biological Molecules. *Journal of Raman Spectroscopy: An International Journal for Original Work in all Aspects of Raman Spectroscopy, Including Higher Order Processes, and also Brillouin and Rayleigh Scattering* **2007**, *38*, 1133-1147.
21. Orendorff, C. J.; Ducey Jr, M. W.; Pemberton, J. E., Quantitative Correlation of Raman Spectral Indicators in Determining Conformational Order in Alkyl Chains. *The Journal of Physical Chemistry A* **2002**, *106*, 6991-6998.
22. Guo, C.; Liu, H.; Wang, J.; Chen, J., Conformational Structure of Triblock Copolymers by Ft-Raman and Ftir Spectroscopy. *Journal of colloid and interface science* **1999**, *209*, 368-373.
23. Czamara, K.; Majzner, K.; Pacia, M. Z.; Kochan, K.; Kaczor, A.; Baranska, M., Raman Spectroscopy of Lipids: A Review. *Journal of Raman Spectroscopy* **2015**, *46*, 4-20.
24. Okabayashi, H.; Okuyama, M.; Kitagawa, T., The Raman Spectra of Surfactants and the Concentration Dependence of Their Molecular Conformations in Aqueous Solutions. *Bulletin of the Chemical Society of Japan* **1975**, *48*, 2264-2269.
25. Holland-Moritz, K.; Hummel, D.-O., Structural Studies on Linear Aliphatic Polyesters by Electron Diffraction, Infrared, and Raman Spectroscopy. *Journal of Molecular Structure* **1973**, *19*, 289-300.
26. Jastrzebska, M.; Wrzalik, R.; Kocot, A.; Zalewska-Rejdak, J.; Cwalina, B., Raman Spectroscopic Study of Glutaraldehyde-Stabilized Collagen and Pericardium Tissue. *Journal of Biomaterials Science, Polymer Edition* **2003**, *14*, 185-197.
27. Brown, G. M.; Hope, G. A., Sers Study of the Adsorption of Gelatin at a Copper Electrode in Sulfuric Acid Solution. *Journal of Electroanalytical Chemistry* **1995**, *397*, 293-300.
28. Leikin, S.; Parsegian, V. A.; Yang, W. H.; Walrafen, G. E., Raman Spectral Evidence for Hydration Forces between Collagen Triple Helices. *Proceedings of the National Academy of Sciences of the United States of America* **1997**, *94*, 11312-11317.
29. Gullekson, C.; Lucas, L.; Hewitt, K.; Kreplak, L., Surface-Sensitive Raman Spectroscopy of Collagen I Fibrils. *Biophysical journal* **2011**, *100*, 1837-1845.
30. Movasaghi, Z.; Rehman, S.; Rehman, I. U., Raman Spectroscopy of Biological Tissues. *Applied Spectroscopy Reviews* **2007**, *42*, 493-541.

31. Frushour, B. G.; Koenig, J. L., Raman Scattering of Collagen, Gelatin, and Elastin. *Biopolymers* **1975**, *14*, 379-391.
32. Zhang, Y.; Mehta, M.; Mansel, B. W.; Ng, H. W.; Liu, Y.; Holmes, G.; Le Ru, E. C.; Prabakar, S., Anion‐Regulated Binding Selectivity of Cr (Iii) in Collagen. *Biopolymers* **2020**, *111*, e23406.
33. Stewart, S.; Fredericks, P. M., Surface-Enhanced Raman Spectroscopy of Peptides and Proteins Adsorbed on an Electrochemically Prepared Silver Surface. *Spectrochimica Acta - Part A: Molecular and Biomolecular Spectroscopy* **1999**, *55*, 1615-1640.
34. Wilson Jr, E. B., The Normal Modes and Frequencies of Vibration of the Regular Plane Hexagon Model of the Benzene Molecule. *Physical Review* **1934**, *45*, 706.